Spatial complexity in dissolved organic matter and trace elements driven by hydrography and freshwater input across the Arctic Ocean during 2015 Arctic GEOTRACES expeditions

Williford, Tatiana; Amon, Rainer M.W.; Kaiser, Karl; Benner, Ronald; Stedmon, Colin; Bauch, Dorothea; Fitzsimmons, Jessica N.; Gerringa, Loes J.A.; Newton, Robert; Hansell, Dennis A.

Total number of authors:
18

Published in:
Journal of Geophysical Research: Oceans

Link to article, DOI:
10.1029/2022JC018917

Publication date:
2022

Document Version
Peer reviewed version

Spatial complexity in dissolved organic matter and trace elements driven by hydrography and freshwater input across the Arctic Ocean during 2015 Arctic GEOTRACES expeditions

Tatiana Williford[1]*, Rainer M.W. Amon[1,2]*, Karl Kaiser[1,2] Ronald Benner[3], Colin Stedmon[4], Dorothea Bauch[5,6], Jessica N. Fitzsimmons[1], Loes J.A. Gerringa[7], Robert Newton[8], Dennis A. Hansell[9], Mats A. Granskog[10], Laramie Jensen[1], Luis M. Laglera[11], Angelica Pasqualini[8], Benjamin Rabe[12], Heather Reader[13], Michiel Rutgers van der Loeff[12], Ge Yan[2]

[1]Texas A&M University, USA
[2]Texas A&M University Galveston Campus, USA
[3]University of South Carolina, USA
[4]Technical University of Denmark, Denmark
[5]Leibniz-Laboratory, University of Kiel CAU, Germany
[6]GEOMAR Helmholtz Centre for Ocean Research, Germany
[7]Royal Netherlands Institute for Sea Research, Netherlands
[8]Columbia University, City of New York, USA
[9]Rosenstiel School of Marine and Atmospheric Sciences, Miami, Florida
[10]Norwegian Polar Institute, Fram Centre, Tromsø, Norway
[11]Universidad de las Islas Baleares, Spain
[12]Alfred- Wegener Institute for Polar- und Marine Research, Germany
[13]Memorial University of Newfoundland, St. John's, Canada

*Corresponding author: Tatiana Williford (Tatiana.Williford@gmail.com), Rainer M.W. Amon (ɐmonr@tamu.edu)

Key Points:

- Dissolved Organic Matter (DOM) distribution in the Arctic Ocean is largely controlled by sea ice formation and melt processes.
- DOM distribution in the Arctic Ocean reveals its potential as a tracer for halocline formation and freshwater source assignments.
- Terrigenous and marine DOM are carriers of trace elements from shelves to the open Arctic Ocean, but terrigenous DOM represent stronger ligands.

This article has been accepted for publication and undergone full peer review but has not been through the copyediting, typesetting, pagination and proofreading process, which may lead to differences between this version and the Version of Record. Please cite this article as doi: 10.1029/2022JC018917.

Abstract

This study traces dissolved organic matter (DOM) in different water masses of the Arctic Ocean and its effect on the distributions of trace elements (TEs; Fe, Cu, Mn, Ni, Zn, Cd) using fluorescent properties of DOM and the terrigenous biomarker lignin. The Nansen, Amundsen, and Makarov Basins were characterized by the influence of Atlantic water and the fluvial discharge of the Siberian rivers with high concentrations of terrigenous DOM (tDOM). The Canada Basin and the Chukchi Sea were characterized by Pacific water, modified through contact with productive shelf sediments with elevated levels of marine DOM. Within the surface layer of the Beaufort Gyre, meteoric water (river water and precipitation) was characterized by low concentrations of lignin and terrigenous DOM fluorescence proxies as DOM is removed during freezing. High-resolution *in situ* fluorescence profiles revealed that DOM distribution closely followed isopycnals, indicating the strong influence of sea-ice formation and melt, which was also reflected in strong correlations between DOM fluorescence and brine contributions. The relationship of DOM and hydrography to TEs showed that terrigenous and marine DOM were likely carriers of dissolved Fe, Ni, Cu from the Eurasian shelves into the central Arctic Ocean. Chukchi shelf sediments were important sources of dCd, dZn, and dNi, as well as marine ligands that bind and carry these TEs offshore within the upper halocline (UHC) in the Canada Basin. Our data suggest that tDOM components represent stronger ligands relative to marine DOM components, potentially facilitating the long-range transport of TE to the North Atlantic.

Plain Language Summary

The Arctic Ocean receives a disproportionate large amount of global river discharge and has limited but well-constrained exchanges with other oceans. This makes the Arctic Ocean unique in terms of dissolved organic matter (DOM) and trace element (TE) sources and distribution. We used data collected during two expeditions spanning the entire Arctic Ocean to characterize the unique distribution of DOM and to study its potential as a water mass tracer and its role in the transport of TE. While the Atlantic-dominated Nansen Basin was characterized by low levels of the DOM and TE, the central Arctic was dominated by the Transpolar Drift, a current that connects the Eurasian shelves to the Fram Strait and transports DOM from the Siberian Rivers towards the North Atlantic. In contrast, the Chukchi shelf-Canada Basin region was characterized by the dominance of Pacific water that is enriched by marine DOM from the shallow and productive Chukchi shelf. The distribution of DOM from these different sources was affected by freezing and thawing processes and, therefore, can be used to study water mass transformations and pathways in the Arctic Ocean.

1. Introduction

Shifts in circulation regimes (Proshutinsky and Johnson, 1997), changes in the freshwater budget due to sea ice decline (Li et al., 2021), and increasing fluvial discharge (Fichot et al., 2013; Ahmed et al., 2020) in the Arctic Ocean are believed to influence the strength of the Atlantic Meridional Overturning Circulation (AMOC) and can have global impacts (Bruhwiler et al., 2021; Zhang et al., 2021; Jiang et al., 2021). State-of-the-art climate models (e.g.,

Proshutinsky et al., 2020, Jiang et al., 2021), remote sensing (e.g., Fichot et al., 2013), and observations (e.g., Yamamoto-Kawai et al., 2009, Guay et al., 2009, Polyakov et al., 2013, Rabe et al., 2014) have focused on the freshwater balance in the Arctic Ocean. In particular, studies have concentrated on the expanding Beaufort Gyre, an anticyclonic system in the Canada Basin that maintains the largest oceanic freshwater reservoir in the Arctic Ocean (Proshutinsky et al., 2019). Freshwater sources include fluvial discharge, Pacific water (which is less saline than Atlantic water), net precipitation, and sea ice melt (Carmack et al., 2008, Haine et al., 2015; Yamamoto-Kawaii et al., 2008; Proshutinsky et al., 2019). Environmental variability is imprinted in the chemical and optical properties of the omnipresent DOM, which makes dissolved organic matter (DOM) a tracer of freshwater sources as well as mixing processes in the ocean.

For example, we use lignin phenols, unique biomarkers of terrigenous DOM (tDOM) in the ocean (Opsahl and Benner, 1997; Opsahl et al., 1999; Benner et al., 2005; Kaiser et al., 2017; Williford et al., 2021), as a tracer of fluvial DOM in the Arctic Ocean. In addition to this terrigenous biomarker (lignin), we use the optical properties of chromophoric DOM (CDOM), including Parallel Factor Analysis (PARAFAC) of fluorescent DOM (Gonçalves-Araujo et al., 2016; Stedmon et al., 2021). Besides the characterization of surface waters of the Arctic Ocean, we are interested in the halocline layers with respect to DOM. In particular, we are interested how DOM can inform about the sources, distribution, and generation mechanisms of Arctic halocline layers and how that affects TE transport.

The Arctic Ocean is an ideal place to study metal-dissolved organic matter (DOM) interactions because it has limited exchanges with other oceans and has abundant sources of DOM and trace elements (TEs) in the upper water column, including fluvial discharge and input from productive shelf regions. Arctic rivers are an important source of both DOM and dissolved

trace metals on the shelves and in the central basins of the Arctic Ocean (Opsahl et al., 1999; Amon 2004; Benner et al., 2005; Krachler et al., 2012; Klunder et al., 2012; Jensen et al., 2020; Benner 2011; Amon et al., 2012; Charette et al., 2020; Williford et al., 2021). Climate change-induced permafrost thaw, tundra greening, and coastal erosion enhance the mobilization of carbon from terrestrial Arctic ecosystems (Fritz et al., 2017; Berner et al., 2020), with a cascading effect on the supply of terrigenous DOM (tDOM) and TEs (Pokrovsky et al., 2012; Berner et al., 2020). Poor understanding of the complex relationships among organic ligands and dissolved trace metals in seawater has limited our ability to predict the magnitude of certain metal fluxes, the spatial extent of their transport away from their source, and the rate of metal scavenging and biological uptake to the particulate phase across a range of metals. In addition to the geochemical and biological factors, other factors like the electron configuration of a trace metal also affect ligand preference through the spatial arrangement of binding sites. For example, iron-ligand associations can range from monodentate to hexadentate complexation (Butler and Theisen, 2010; Williford et al., 2021). Molecular size also impacts the binding strength of ligands, with higher-molecular-weight molecules typically having a greater number of binding sites, more flexible molecular geometries, and greater binding strength (Laglera & van den Berg 2009; Williford et al., 2021).

In this study, we explore the potential of DOM as a tracer of river discharge, freezing/thawing processes, and water mass pathways using biomarker lignin and examining the optical properties of CDOM. We characterize prominent Arctic features like the Beaufort Gyre, Transpolar Drift (TPD), upper and lower haloclines (UHC, LHC) in terms of DOM concentration and origin. Additionally, we examine potential links between hydrography, diverse

groups of DOM molecules and several dissolved trace metals (dFe, dMn, dNi, dCu, dZn, dCd) across the breadth of the Arctic Ocean.

2. Materials and Methods

2.1. Hydrographic Context

Discrete water samples, *in situ* CDOM fluorescence, and hydrographic data were collected in the summer of 2015 during the U.S. Arctic GEOTRACES (GN01) cruise aboard the USCGC *Healy* (HLY1502) and the GEOTRACES TransARC II cruise (PS94) on the German research icebreaker *Polarstern* (Fig. 1; Rabe et al., 2016a, 2016b; Schauer, 2016). The GN01 cruise track (August 9th to October 12th 2015; Kadko and Landing, 2015) consisted of a "northbound" transect along ~170°-180° W stretching through Bering Strait and across the Canada and Makarov Basins to the North Pole (GN01 stations 1–32), and the "southbound" transect returning southward along ~150°W across the Makarov and Canada Basins back into Chukchi shelf waters (GN01 stations 33–57). The PS94 cruise track (August 17th to October 15th; Schauer, 2016) consisted of 2 transects extending from the Barents Sea and the Gakkel Ridge, respectively, into the Makarov Basin. The CTD data can be found at the PANGAEA data archive (https://www.pangaea.de: https://doi.org/10.1594/PANGAEA.859558), the British Oceanographic Data Centre (http://www.bodc.ac.uk/geotraces), and Biological and Chemical Oceanography Data Management Office (Landing et al., 2019a, 2019b).

The U.S. GEOTRACES GN01 and the TransARCII PS94 missions included two inter-calibration stations. Data from the North Pole station were collected synchronously (PS94 station 87, corresponding to GN01 station 32), while those from the deep Makarov Basin at 87°30'N 180°E (PS94 station 101, corresponding to GN01 station 30) were collected two weeks apart.

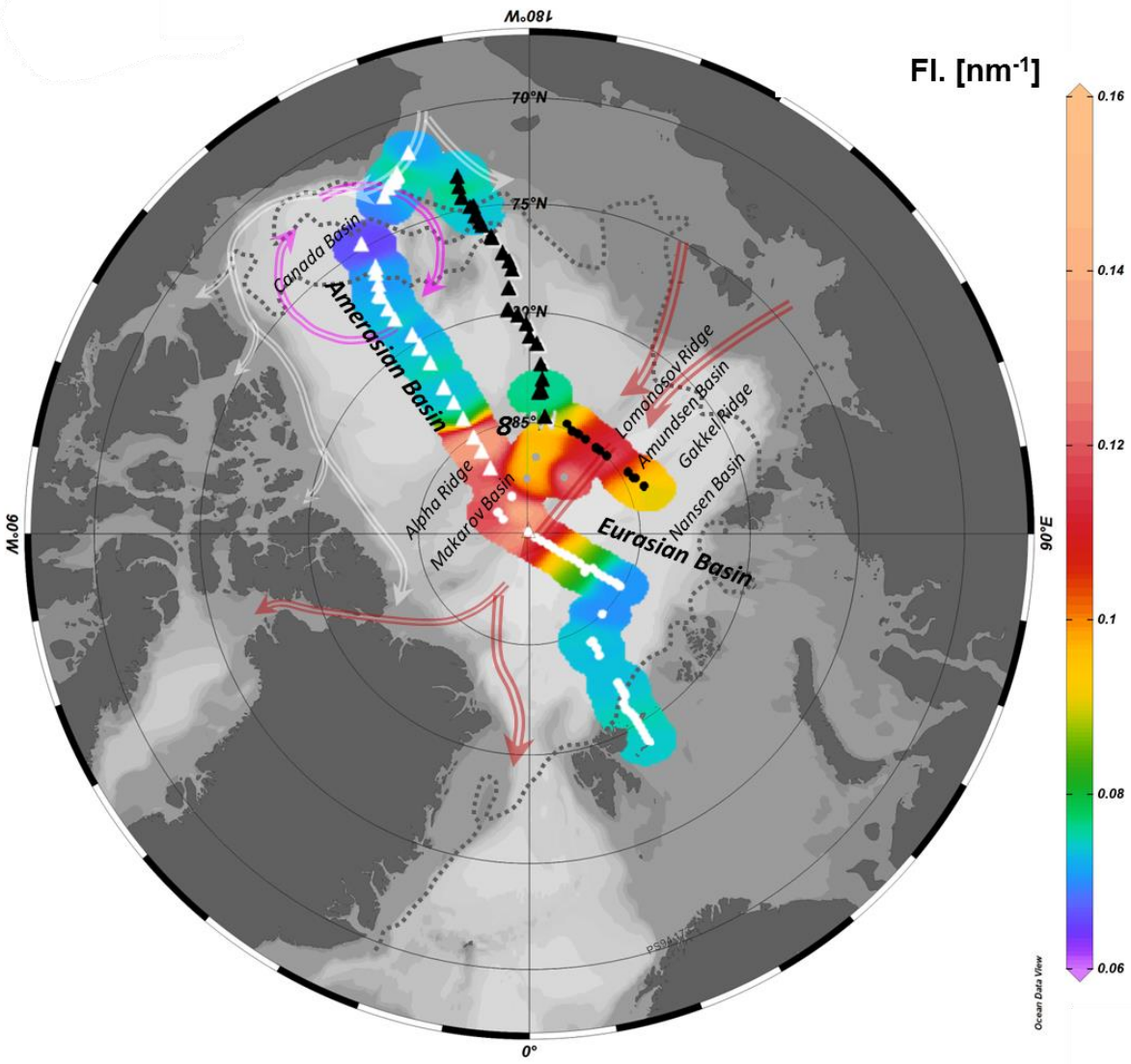

Figure 1. The U.S. GEOTRACES Arctic GN01 transect cruise track (triangles) and the TransARCII PS94 cruise track (squares). The approximate locations of major upper ocean circulation features are shown in grey, red (Transpolar Drift), and magenta (Beaufort Gyre). Surface *in situ* CDOM fluorescence (Fl.) in surface waters is shown in color (in nm^{-1}), extrapolated out to 100 km for visualization purposes. The grey dotted line indicates the sea ice edge at the time of sampling (August 2015, NSIDC database, 2015). Section A is shown in white symbols; section B is shown in black symbols. *In situ* CDOM fluorescence was not measured along most of the Amerasian Basin portion of section B. This figure and section plots in the manuscript were generated using Ocean Data View (Schlitzer, 2020).

Here we define Section A (white symbols, Fig.1) as stretching from the Chukchi Sea shelf, across the North Pole (GN01 stations), and through the Amundsen and Nansen Basins to the Barents Sea (PS94 stations). The following hydrographic distinctions of water masses were assigned. The thickness of the relatively fresh polar mixed layer (PML,S<31) is conventionally defined by the temperature minimum (Rudels et al., 1996). However, in cases where the temperature minimum cannot be identified with certainty, the rapid change in magnitude of the salinity gradient may be used (Korhonen et al., 2013). For example, the Chukchi Sea and southern Canada Basin are strongly influenced by seasonal sea ice melt, resulting in a near-surface temperature maximum from radiative warming of surface waters during summer (Shimada et al., 2001. Jackson et al., 2010). The average depth of winter convection is about 45m in the northern Canada Basin and 35m in the southern Canada Basin (Korhonen et al., 2013). In the Amundsen and Makarov basins, the PML deepens to about 55 m, becomes shallower, and occupies a depth of 40 to 50 m in the Nansen Basin (Rudels, 2009; Korhonen et al., 2013).

In the Canada Basin, underneath PML lies the upper halocline (UHC), in the Canada Basin largely derived from Pacific water. Because of its origin, the boundary between the upper and the lower haloclines is roughly defined by the isohaline of S = 34 (Korhonen et al., 2013). The Beaufort Gyre is a large anticyclonic system in the surface layer of the Canada Basin, marked by low salinity and low *in situ* CDOM fluorescence (Fig.1). Shelf-waters within the UHC and lower halocline (LHC) are pushed downward by convergence associated with Ekman forcing in the surface Beaufort Gyre (Watanabe, 2013). According to climatology (Korhonen et al., 2013), the UHC is the thickest (180-200m) in the southern Canada Basin. In the Makarov and

Amundsen Basins, the thickness decreases to 40m and 30m, respectively, and in the Nansen Basin, the UHC is generally absent (Korhonen et al., 2013). The LHC thickness in the Canada Basin varies between 60 and 70m and increases towards the central Arctic Basins (~80m in the Amundsen and Makarov Basins) and becomes thinner, < 50m, in the Nansen Basin (Korhonen et al., 2013). The Atlantic Water (AW; S>34.7; Rudels et al., 2001) beneath the haloclines transitions into dense (σ>28 kg/m^3) deep water (DW) below 1000m depth.

Section B (black symbols, Fig. 1) is closer to the Eurasian slope and consists of the "northbound" leg of the GN01 cruise and the PS94 cruise transect between stations 117 and 134. Unfortunately, *in situ* CDOM fluorescence was not measured along most of the Amerasian Basin portion of section B (Fig. 1). Like section A, section B crossed the Amundsen and Makarov Basins, where the TPD can be observed by elevated surface *in situ* CDOM fluorescence.

2.2. Optical properties of DOM

Water samples collected for absorption and fluorescence analyses were filtered through a 0.2 µm Millipore filter cartridge attached to Niskin bottles mounted on a CTD rosette. CDOM fluorescence was measured by two independent approaches. An *in situ* approach using backscatter fluorescence sensors with a broadband excitation of 350-460 nm and 550±20 nm emission. The two instruments used on the ships were intercalibrated using the method introduced and discussed in Stedmon et al. (2021). The fluorescence intensities at excitation 350 and emission 450 nm measured in the water samples collected onboard at the same time were used to calibrate the voltage signal from the CTD-mounted Dr. Haardt fluorometers.

The second approach to determine CDOM fluorescence was a laboratory measurement of collected water samples using a bench-top spectrofluorometer. For the PS94 portion of the

samples, Horiba Aqualog spectrofluorometer was used, and the details for the fluorescence measurements are described in Stedmon et al. (2021). For the GN01 portion, 132 samples were collected for DOM fluorescence measured using a Photon Technologies International spectrofluorometer (Quanta Master-4 SE) with a 1 cm quartz cuvette. Excitation-emission matrix scans (EEMs) for each sample covering emission from 280 to 600 nm (2 nm increment) and excitation wavelengths ranging from 220 to 450 nm (5 nm increment). Daily pure water (Milli-Q®) blanks were obtained and subtracted to remove water scattering peaks. Data were spectrally corrected for instrument bias, and subsequently, Raman calibrated (excitation 350 nm) using the pure water blanks and the drEEM toolbox (version 0.2.0, Murphy et al., 2013). The Dr. Haardt signal was linearly correlated to the excitation 350 nm and emission 450 nm signal measured by the laboratory spectrofluorometer (Fig. S1) to correct for the offset between the 2 sensors as described in Stedmon et al., (2021).

Studies show that not all of the instrument bias is removed using the manufacturer's spectral correction procedures (Cory et al., 2010). This problem is particularly important when multivariate data analyses will be applied. To circumnavigate the potential minor spectral differences, the datasets collected using different instruments were analyzed separately. Excitation below 250 nm was not included due to excessive instrument noise resulting from poor lamp output.

Two PARAFAC models were developed for the EEMs data: a four-component model was developed for the GN01 data set (C1) and a six-component model for the PS94 data set (C2). The four-component model (C1) was optimized based on spectral loadings, residual examination, and split-half validation using a convergence criterion of $1e^{-8}$ (Fig. S2a). The components were labeled based on their emission maxima: $C1_{482}$, $C1_{428}$, $C1_{402}$, $C1_{348}$. For the

EEMs from the PS94 cruise, a six-component model (C2) was optimized based on spectral loadings, residual examination, and split-half validation using a convergence criterion of $1e^{-8}$ (Fig.S2b). The components were labeled based on their emission maxima: $C2_{411}$, $C2_{456}$, $C2_{404}$, $C2_{492}$, $C2_{338}$, and $C2_{302}$.

The spectral characteristics of each component were compared to those from several previous studies using the OpenFluor database (Murphy et al., 2014; Table S1, S2).

2.3 Lignin phenols analysis

The sum of concentrations of nine lignin phenols (TDLP9) is reported in this study, including p-hydroxyls (p-hydroxybenzaldehyde, p-hydroxy acetophenone, p-hydroxybenzoic acid), vanillyls (vanillin, acetovanillone, vanillic acid), and syringyls (syringaldehyde, acetosyringone, syringic acid). To measure the lignin phenols, unfiltered seawater samples containing 30 µg of DOC were acidified to pH 2.5 using concentrated HCl (reagent grade) and extracted onto 1 g reversed-phase (C18) sorbent cartridges using a Dionex Autotrace 280 Solid-Phase Extraction instrument. Lignin phenol analysis was performed following the method of Yan and Kaiser (2018 a, b). It allows the quantification of dissolved lignin phenols in small volumes of seawater (<200 mL) using alkaline $CuSO_4$ at 150°C. Ultra-high performance liquid chromatography with mass spectrometry detection in dynamic Multiple Reaction Monitoring mode and isotopically labeled surrogate standards were used for the detection and quantification of monomeric lignin phenols.

2.4. Dissolved organic and inorganic carbon

DOC concentrations were determined using a Shimadzu TOC- L, according to Halewood et al. (2010); all samples were filtered at the time of collection using 0.2 μm pore size. The data are available online (Hansell, 2017; 2021). The accuracy was confirmed by measuring deep-water standards from the Consensus Reference Waters (Hansell, 2005). DOC measurements from both cruises (GN01 and PS94) were done at the Rosenstiel School of Marine & Atmospheric Sciences, University of Miami; they were consistent at the crossover stations.

Dissolved inorganic carbon (DIC) concentrations were measured using the methods of Woosley et al. (2017) and Ulfsbo et al. (2018). A description of the two cruises and the uncertainty analyses were discussed in Charette et al. (2020).

2.5 Trace metal data

Dissolved Fe and other TE data were obtained from Jensen et al. (2019) for GN01 Zn, Zhang et al. (2020) for GN01 Cd, Jensen, et al. (2019, 2020, 2022) for GN01 Fe and Mn, Gerringa et al., (2021) for GN04 trace metals, and Jensen (2022) for GN01 Cu and Ni. Sample collection and analyses followed GEOTRACES protocols (Cutter et al., 2010; Rijkenberg et al., 2018).

2.6 Linear mixing model

To study the pathways of DOM and TEs in the Arctic Ocean, the fractions of seawater with Pacific (f_{Pac}) and Atlantic (f_{Atl}) origin, sea ice melt (f_{SIM}), and meteoric water (f_{Met}) were determined based on the salinity (S), $\delta^{18}O$- H_2O (stable oxygen isotope ratio in water), and the Arctic N- P tracer (ANP, Newton et al., 2013). Mass balance for total mass and these four tracers are combined into the following system of linear equations, which is solved for each sample:

$$f_{Pac} + f_{Atl} + f_{SIM} + f_{Met} = 1 \quad (1)$$

$$f_{Pac}[S_{Pac}] + f_{Atl}[S_{Atl}] + f_{SIM}[S_{SIM}] + f_{Met}[S_{Met}] = [S]_{measured}, \quad (2)$$

$$f_{Pac}[\delta^{18}O_{Pac}] + f_{Atl}[\delta^{18}O_{Atl}] + f_{SIM}[\delta^{18}O_{SIM}] + f_{Met}[\delta^{18}O_{Met}] = [\delta^{18}O]_{measured}, \quad (3)$$

$$f_{Pac}[ANP_{Pac}] + f_{Atl}[ANP_{Atl}] + f_{SIM}[ANP_{SIM}] + f_{Met}[ANP_{Met}] = [ANP]_{measured} \quad (4)$$

'Meteoric' water is a combination of runoff and in situ precipitation. 'Sea ice melt' is the net meltwater fraction, and does not distinguish between sequential passage into and out of the solid phase. Negative SIM is associated with net sea ice formation (i.e.: the fraction of freshwater extracted from a seawater parcel into the solid phase). The end-member (water sources) values used in the calculations are presented in Table 1. The isotope data were from Pasqualini et al., (2017) and Paffrath et al., (2021). The limitations of the method and choices of end-members are discussed in detail in Newton et al. (2013) and Charette et al. (2020). We note here that the most significant errors in the method are known to be in the separation of Atlantic and Pacific water masses, which rely on nutrient combinations that are only quasi-conserved in the near-surface ocean. Current discussions of these issues, and novel suggestions for improvement, can be found in Alkire et al. (2018), Paffrath, et al. (2021), and Whitmore, et al. (2020). High fractions of Pacific water in the TPD may actually originate from within the Chukchi and Siberian shelves instead (Bauch et al., 2011). Novel results based on rare earth elements concentrations and Nd isotopes confirm this assumption (Paffrath et al., 2021) and show that high Pacific water fractions in the TPD (Fig. 2) can be an error of the method.

Table 1. End-member values used in mass balance calculations (from Newton et al. 2013)

Water Mass	Salinity	δ^{18}O [‰]	Arctic N:P (ANP)
Atlantic (Atl)	34.92	0.3	0

Pacific (Pac)	32.5	-1.1	1
Meteoric (Met)	0	-19	0
Sea-ice melt (SIM)	4	surface +2.6	surface

3. Results

3.1 Water fractions

The four basic water fractions identified for the Arctic Ocean (Atlantic water, Pacific water, meteoric water, and sea-ice melt water), based on salinity, $\delta^{18}O$, and the ANP (Newton et al., 2013), indicated that up to 95% of the water in the central Nansen Basin originated from the Atlantic Ocean (Fig. 2). In the Canada, Makarov and Amundsen Basins, AW occupied depths underneath the Pacific Water (PW) layer, while PW dominated the top 100-250 meters (Fig. 2). The distribution of AW and PW in the TPD was not correctly reflected by the ANP method alone and erroneously overrepresented the Pacific component (Paffrath et al., 2021). The Beaufort Gyre convergence results in a deepening of the upper boundary of the AW in the Canada Basin and its shoaling in the Makarov Basin (Zhong and Zhao, 2014). The border between the UHC and LHC roughly corresponded to the isopycnal of 27 kg/m^3 (where f_{Pac} and f_{Atl} each account for ~50% of water), which was also the density surface of the *in situ* CDOM fluorescence maximum (Fig. 3, S3).

Sea-ice melt water (f_{SIM}) constituted 5% of the PML in the Canada and Nansen Basins. A brine signal (negative f_{SIM}) was detected within the TPD system and the upper 100 meters of the Makarov and Amundsen Basins. According to the computed fractions, the halocline layers were also affected by brine formation. The PML shows great variation in the sea-ice meltwater fraction (f_{SIM}), along sections A and B, and between the two, with f_{SIM} ranging from –8% to

+7%. In both the upper and lower halocline waters sea-ice formation (brine enrichment, negative f_{SIM}) dominated, with f_{SIM} being more negative in the upper than the lower layer (Fig. 2). The PML in the Canada, Makarov, and Amundsen Basins exhibited a significant (up to ~22%) contribution of meteoric water (f_{Met}). The surface waters of these basins are strongly influenced by the TPD, which carries freshwater from the Siberian shelves. In addition to river discharge, the water mass calculations indicated that these waters had experienced ice melt, ice formation, and brine rejection.

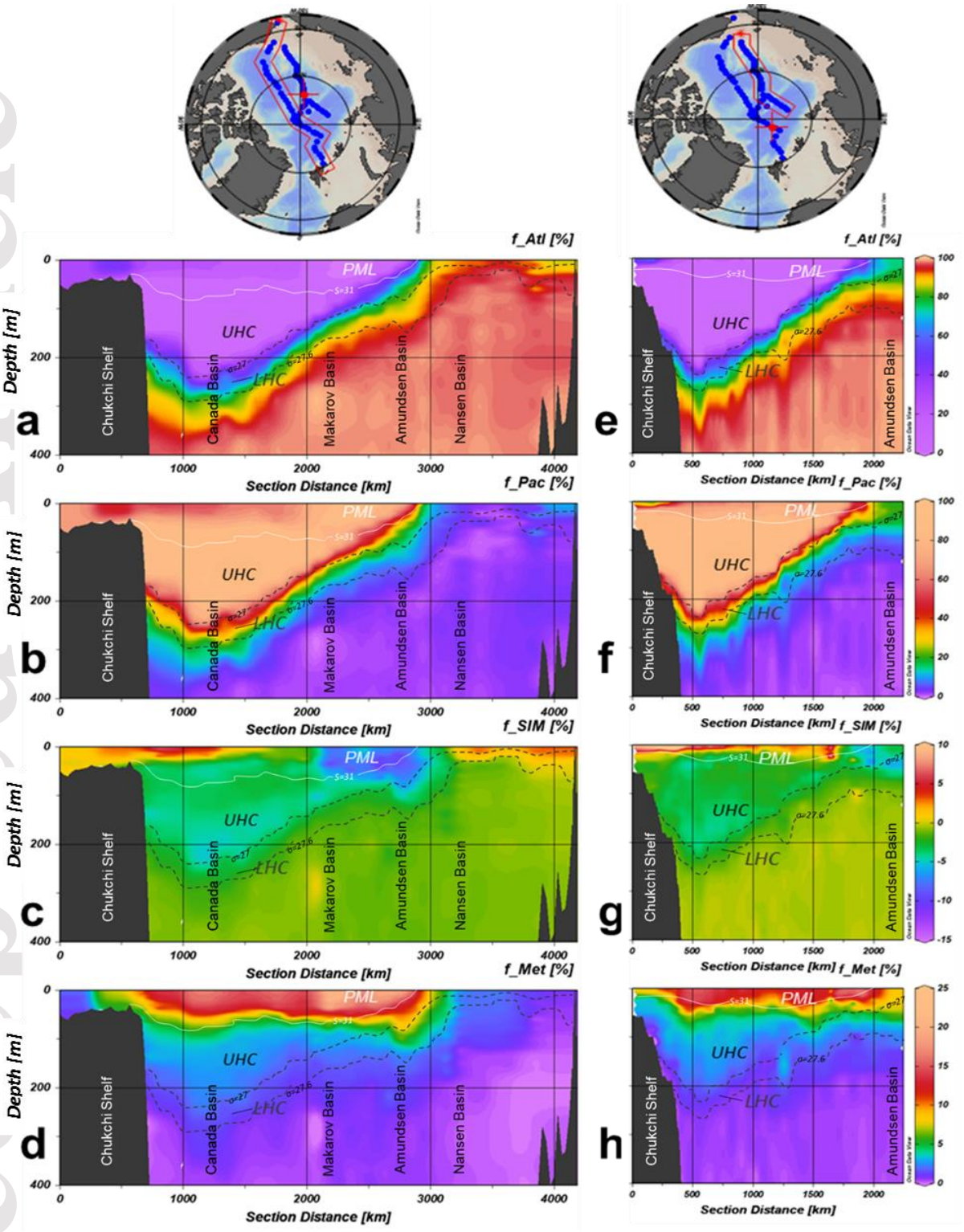

Figure 2. Calculated fractions of f_{Atl}, (a, e), f_{Pac} (b, f), f_{SIM} (c, g) and f_{Met} (d, h) for sections A and B, respectively. The white line represents the isohaline of S=31, which is the border of the polar

mixed layer (PML) in the Canada Basin. Black dashed isopycnal of $\sigma = 27$ kg/m^3 represents the lower/upper halocline (LHC/UHC) border. The LHC is bordered at the bottom by the isopycnal of $\sigma = 27.6$ kg/m^3. The color bar scales are different in each panel.

3.2 CDOM fluorescence

In situ CDOM fluorescence was highly variable in the different Arctic Ocean basins (Fig. 3), especially within the upper 400 m of the water column, but showed a very distinct pattern. Starting from the east, CDOM was consistently low throughout the water column of the Nansen Basin (<0.01 nm^{-1}; Fig. 3). In the Central Arctic, the hydrography of the surface waters are governed by the TPD circulation, and the upper 70 meters are characterized by very high *in situ* CDOM fluorescence (~0.08 nm^{-1}; Charette et al. 2020). The elevated fluorescence signal can be traced to a depth of 210 meters in the Makarov and Amundsen Basin and to about 180 meters above the Lomonosov ridge (Fig. 3).

In contrast, in the Western Arctic, the *in situ* CDOM fluorescence was very low in surface waters of the Canada Basin (<0.01 nm^{-1}), but elevated deeper in the UHC and LHC, consistent with previous studies (e.g. Shen et al. 2016; Gao and Guéguen 2018). A maximum in *in situ* CDOM fluorescence was detected at the UHC/LHC interface (roughly corresponding to the isopycnal σ=27 kg/m^3, Fig. 3), about 50 meters below the UHC core as defined by the depth of the nutrient maximum (Fig. 3, S3e). The LHC was also characterized by elevated *in situ* CDOM fluorescence compared to the underlying AW (Fig. 3 a,b). The *in situ* CDOM fluorescence signal closely follows the density structure in the water column, e.g., isopycnal of σ~27.6 kg/m^3 coincided with the lower border of the CDOM trace (Fig. 3).

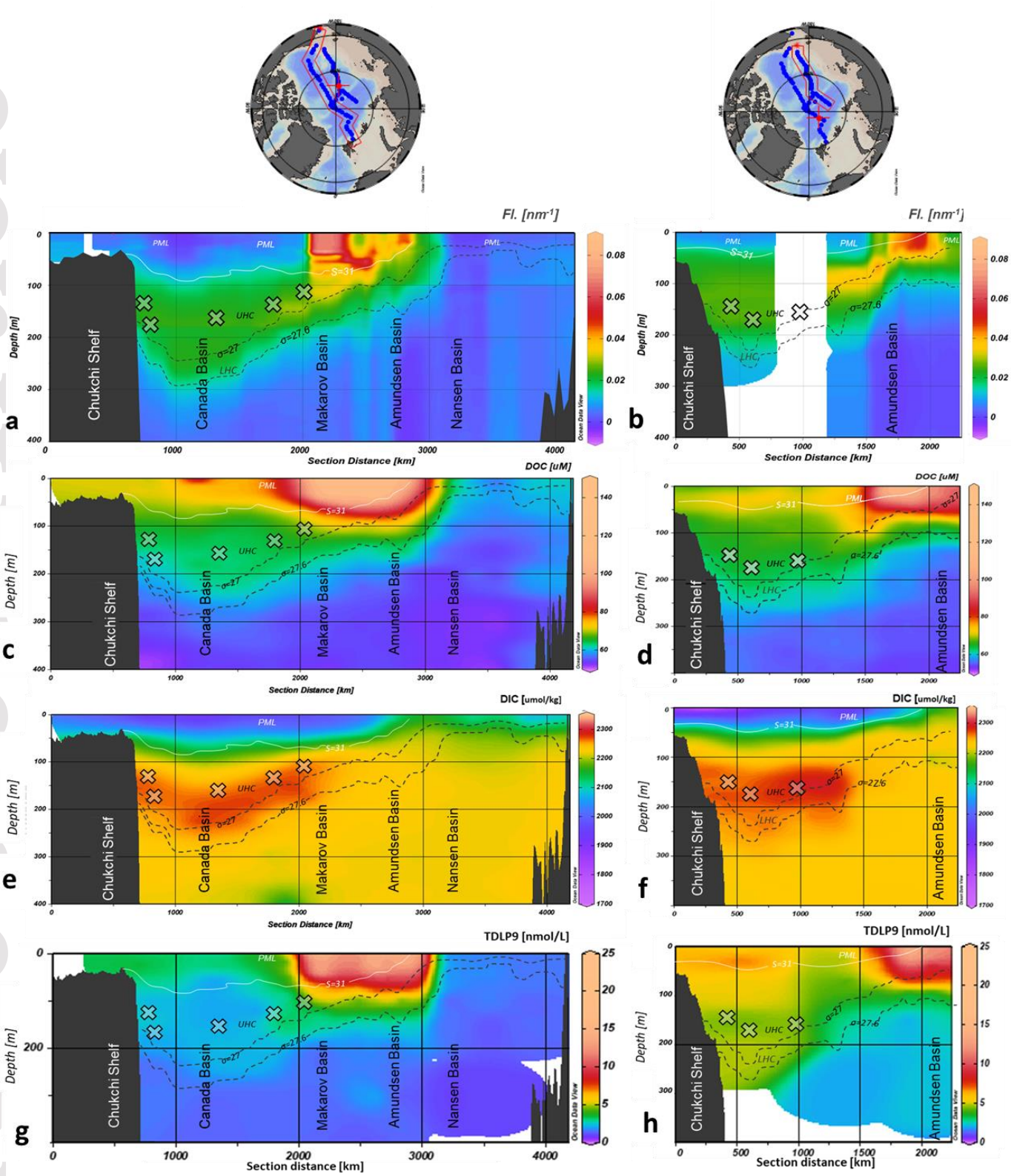

Figure 3. *In situ* CDOM fluorescence (Fl.; a, b), dissolved organic carbon (DOC; c, d), dissolved inorganic carbon (DIC, e, f) and lignin phenols (TDLP9; g, h) concentrations for sections A (a, c, e, g) and B (b, d, f, h) in the upper 400 m. The white line represents the isohaline of S=31, which is the border of the polar mixed layer (PML) in the Canada Basin. Black dashed isopycnal of σ = 27 kg/m^3 represents the upper/lower halocline (LHC/UHC) border in the Canada Basin. The LHC is bordered at the bottom by the isopycnal of σ = 27.6 kg/m^3 in the Canada Basin. The silicate maximum (𝕏) marks the core of the UHC according to Anderson et al. (2013). The color bar scales are different in each panel.

3.3 Dissolved organic carbon

Similar to *in situ* CDOM fluorescence, total DOC concentrations were low throughout the water column (48-63 µmol/L) in the Nansen Basin (Fig. 3). Within the TPD region, DOC concentrations were higher (up to 138 µmol/L) but limited to <170 meters in the Amundsen Basin. In the Canada Basin, the distribution of DOC concentrations was different from CDOM. The former was enriched in the surface of the central Canada Basin (42-73 µmol/L) and decreased with depth. In contrast to CDOM, the DOC concentration was not elevated within the halocline. Below the halocline, AW had low CDOM and low DOC. Surface waters of the Canada Basin in section B (which is closer to the Eurasian shelves) had more DOC than section A by ~7 uM.

3.4 Dissolved inorganic carbon

DIC concentrations were very low at the surface (<1950 µM; Fig. 3), similar to *in situ* CDOM fluorescence (except without the TPD maximum), and enriched in the UHC (up to ~2300 µM). The maximum concentrations of DIC generally coincided with the nutrient maximum marking the core of the UHC (Fig. 3). Within the TPD, the trend was the opposite to *in situ*

CDOM fluorescence, as the surface of the Makarov and Amundsen Basins was depleted in DIC (~1960 μM). The Atlantic inflow in the eastern Arctic had higher DIC than the Pacific inflow at the Chukchi shelf (Fig. 3).

3.5 Lignin phenols

The high salinity (>34.7) waters of Atlantic origin dominating the eastern Arctic's Nansen Basin were characterized by low concentrations of lignin phenols (<3 nmol/L; Fig. 3). In the Central Arctic, the importance of terrigenous DOM within the TPD was confirmed by the high lignin phenol concentrations (up to 21 nmol/L). In the Canada Basin, the vertical gradient was different for the distributions of DOM fluorescence and total DOC concentrations. Lignin phenol concentrations reached 5 nmol/L at the surface of the Canada Basin, decreased within the UHC, and were slightly enriched at the UHC/LHC interface. In general, section B was characterized by higher lignin concentrations than section A (Fig. 3); overall, lignin phenol concentrations were ~5 nmol/L higher in section B, closer to the Eurasian shelves.

3.6 Fluorescent components of DOM

Based on the laboratory spectrofluorometric measurements, two PARAFAC models were developed: a four-component model for the GN01 data set (Canada Basin, C1) and a six-component model for the PS94 data set (Amundsen, Makarov and Nansen Basins, C2). Of all the fluorophores observed in the Canada Basin in this study, component $C1_{482}$ was earlier described as an ideal terrigenous tracer, e.g. in Arctic boreal lakes (Kothawala et al., 2014) and the Arctic Ocean (Walker et al., 2009; Williford et al., 2021). In the Canada Basin, $C1_{482}$ had the strongest correlation with lignin phenol concentrations, confirming its terrigenous origin. The maximum

$C1_{482}$ fluorescence was observed at the very surface of the Canada Basin and in the upper halocline. Component $C1_{434}$ previously identified as marine humic (Kothawala et al., 2014), was highly correlated with DOC and lignin phenol concentrations (Fig. 4).

$C1_{402}$, another humic-like component, has been observed spreading from the Chukchi Sea shelf to the core of the UHC in the Canada Basin and likely originates from marine organic matter decomposition in surface sediments on the shelf (Chen et al., 2018). The distribution of the only protein-like component $C1_{348}$ in the Canada Basin was like that of $C1_{402}$, but with a more pronounced fluorescence signal closer to the Chukchi Sea shelf.

Among all the fluorophores identified in the Nansen, Amundsen, and Makarov Basins, components $C2_{411}$, $C2_{456}$, $C2_{404}$, and $C2_{492}$ were humic-like, while $C2_{338}$ and $C2_{302}$ had a protein-like signature. $C2_{411}$ had the highest fluorescence intensity and is usually suggested to be produced in the water column (Yamashita et al., 2013). The two fluorescent components, $C2_{456}$ and $C2_{492}$, are usually described to be of terrigenous origin (Yamashita et al., 2013; Kothawala et al., 2014, Williford et al., 2021). These components had the strongest correlations with lignin phenol concentrations (Fig. 4). $C2_{456}$ is commonly found in the Arctic Ocean and was reported in surface waters of the central Arctic, close to the Mackenzie River mouth and the Amundsen Gulf (Guéguen et al., 2015), and in the Lena River (Gonçalves-Araujo et al., 2015). $C2_{492}$ has a longer emission wavelength than $C2_{456}$, indicating molecules with higher molecular weight and higher hydrophobicity (Helms et al., 2008). Relative to $C2_{456}$, $C2_{492}$ has a higher molecular weight and therefore is more prone to flocculation, and its fluorescence intensity in the TPD region and the lower halocline was lower but relatively higher on the shelf. $C2_{492}$ fluorescence co-varied with dFe in boreal lakes (Kothawala et al., 2014). Similar to $C1_{402}$, the fourth humic component (third by intensity), $C2_{404}$, resembled a fluorescence signal that had been observed near the Chukchi

Sea shelf and in the core of the upper halocline in the Canada Basin (Chen et al., 2018; Williford et al., 2021). The tryptophan-like $C2_{338}$ and the tyrosine-like $C2_{302}$ components have been reported in Arctic surface waters (Stedmon et al., 2011b; Chen et al., 2018; Williford et al., 2021). Previously, $C2_{338}$ was reported as related to sea-ice CDOM and brine concentration (Stedmon et al., 2011b). The tyrosine-like $C2_{302}$ was reported to be derived partly from the shelf and slope sediments (Chen et a. 2018).

In the Amundsen and Makarov basins, PARAFAC components $C2_{411}$ and $C2_{456}$ dominated the fluorescence signal in the PML and the upper and lower haloclines of the Makarov basin. $C2_{338}$ and $C2_{492}$ were slightly elevated in the PML and the halocline. $C2_{411}$ and $C2_{338}$ had the highest fluorescence intensity in the PML, while terrigenous $C2_{456}$ and $C2_{492}$ were most elevated at about 20 m depth at the upper boundary of the upper halocline.

The fluorescence intensity of all PARAFAC components was low in the Nansen Basin. The protein-like components were slightly elevated at the surface of the northern Nansen Basin (Amundsen Basin side). The Svalbard slope was also characterized by a slight increase in the fluorescence intensity of all the components.

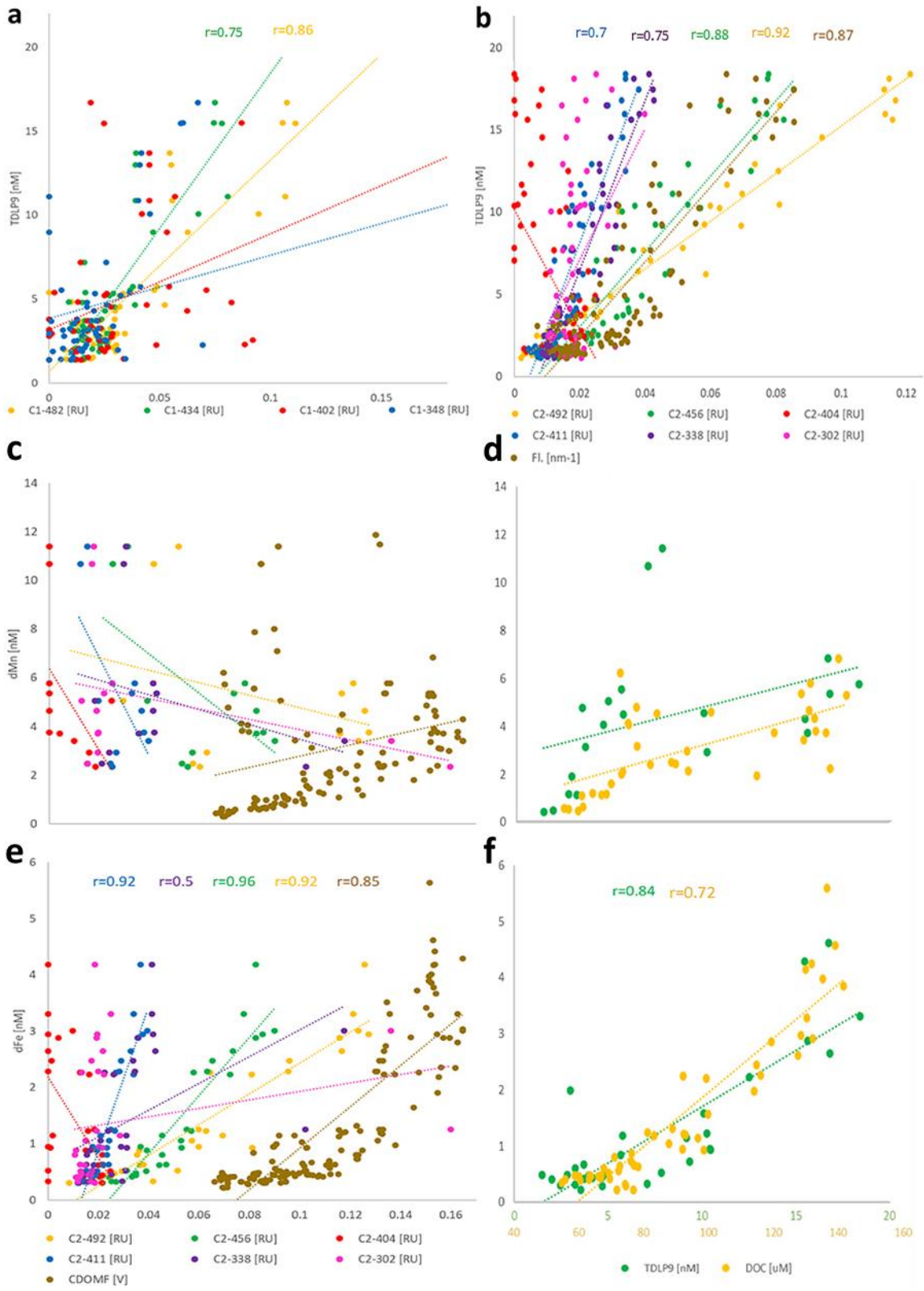

Figure 4. Correlation plots between the lignin phenol concentrations and C1 PARAFAC components (a), C2 PARAFAC components, and *in situ* CDOM fluorescence (Fl.) (b),in the top 300 meters of the Arctic Ocean. Scatterplots between the dMn (c, d), dFe (e, f), and C2 PARAFAC components and *in situ* CDOM fluorescence (CDOMF; c, e), lignin phenols (TDLP9) and dissolved organic carbon (DOC; d, f), in the top 300 meters of the Arctic Ocean. Only significant correlations ($p<0.001$ are shown).

3.7 Trace metals

The TE distributions in the GN01 and GN04 Arctic GEOTRACES sections have been presented previously (Jensen et al., 2019, 2020; Zhang et al., 2019; Gerringa et al., 2021)). In this manuscript, we focus on potential relationships between the TEs and the various types of DOM indicators. The dFe, dNi, and dCu, concentrations in the surface waters of the TPD region were high compared to those in the Canada BasinsBasin (Fig. 5)), and they showed strong to moderate correlations with lignin phenol concentrations, as well as optical indicators of terrigenous DOM ($C1_{482}$, $C2_{492}$; Fig. 4, S7). Other trace metals (dZn, dMn, dCd) did not exhibit correlations with the tDOM indicators.

In the Canada Basin, the PML was enriched in dNi, dCu, dCd, and dMn (Fig. S7). Dissolved Cu was the only trace metal to show a significant correlation with DOC concentrations and protein-like fluorescence in the topupper 300 meters of the Canada Basin (Fig. S7). Interestingly, the correlation between f_{Met} and dCu was strong, but there was no significant correlation between dCu and CDOM.

The upper halocline waters were enriched in the dZn, dNi, dCu and dCd. These metals showed moderate correlations with optical sediment signal. The scavenging-prone dFe and dMn are rapidly lost, moving away from the continental slope (Fig. S5, S6, Jensen, et al. 2020).

Dissolved Fe exhibited weak to absent complexation to degraded UHC marine DOM in the UHC.

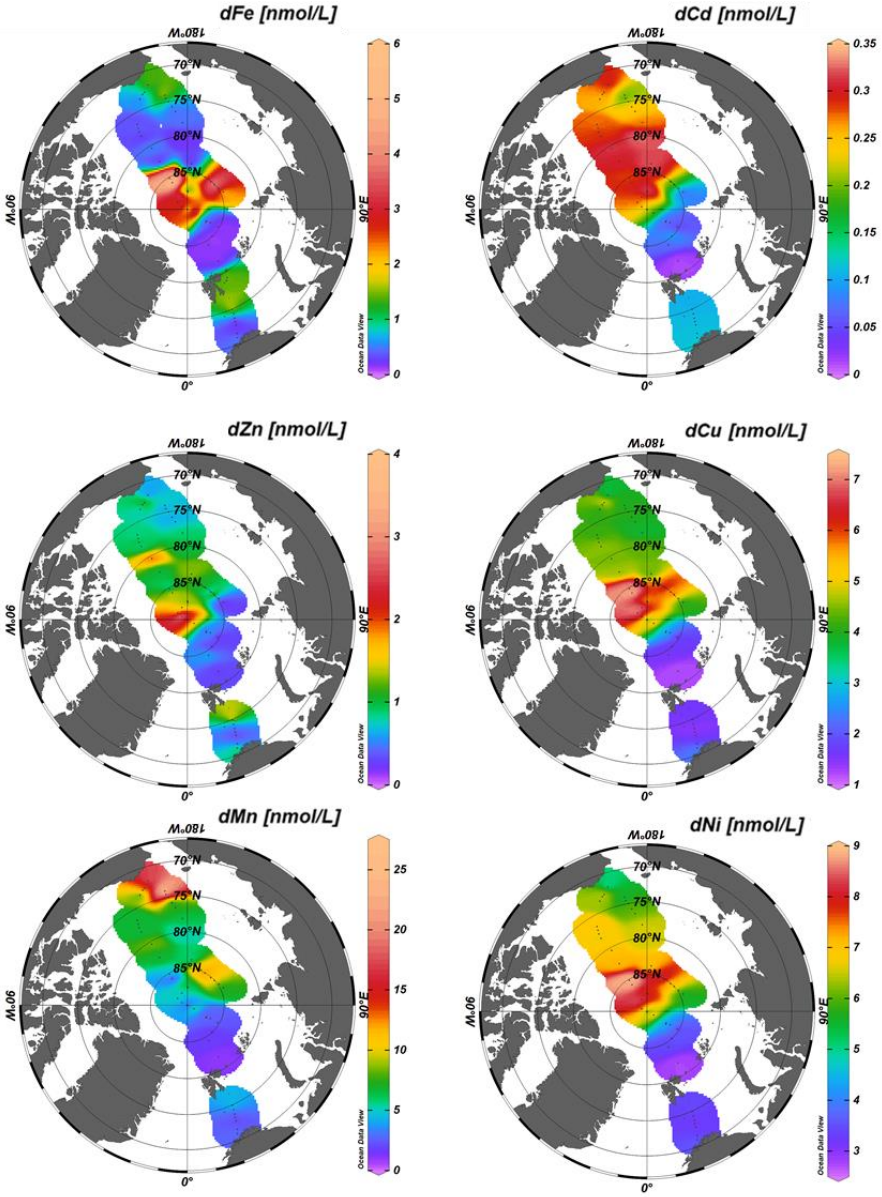

Figure 5. Concentrations of dFe, dMn, dNi, dCu, dZn, dCd in surface sample. The TE distributions data for the GN01 and GN04 Arctic GEOTRACES sections have been published previously (Jensen et al., 2019, 2020; Zhang et al., 2019; Gerringa et al., 2021).

4. Discussion

We characterize the surface Arctic Ocean into three geographic regions based on the distribution of DOC, lignin, and optical properties. These three regions are physically separated by circulation and experience different sources of organic matter. The Eastern Arctic's Nansen Basin/Atlantic Eurasian shelf region is strongly influenced by AW and north-flowing Eurasian shelf waters carrying significant quantities of freshwater, nutrients, DOM, and sediments into the Arctic Ocean (Sholkovitz et al., 1981; Walker et al., 2013; Rudels 2015; Holmes et al., 2019). The buoyant, low-salinity fluvial discharge mixed with the Atlantic water creates an upper ocean flow from the shelves to the central Arctic Ocean (Rennermalm et al., 2006). Arctic shelf waters are diverted by the Coriolis force to form a circumpolar anti-clockwise current shaped by coastal geometry resulting in multiple branches (Carmack et al., 2016; Horner-Devine et al., 2015).Below these upper waters is the lower halocline, which is believed to be formed via two mechanisms: a convective formation implying salinification of cold and fresh surface water and melting of sea ice as Atlantic water enters the ice-covered Arctic shelves, and an advective formation involving the cold and saline shelf water spreading into the deep Arctic basins (Kikuchi et al., 2004; Metzner et al., 2020).

The second region is the central Arctic thatthat consists of the Amundsen and Makarov basins. In these basins, DOM distributions are influenced by the TPD, which connects the Eurasian shelves to the Fram Strait through surface advection (Charette et al., 2020). A clear terrigenous DOM signature is known to characterize the TPD region (Opsahl et al., 1999; Amon, 2004; Slagter et al., 2019; Paffrath et al., 2021; Williford et al., 2021).

On the Western Arctic's side of the TPD, the Chukchi shelf and Canada Basin are influenced by the advection of the relatively fresh (S<33) nutrient-rich waters from the Pacific (Woodgate et al., 2012), which are modified on the shallow Chukchi shelf by the exchange with sediments

(Nakayama et al., 2011; Nishimura et al., 2012; Kondo et al., 2016). Concentrations of terrigenous DOM and CDOM are much lower compared to the Eurasian Arctic and the TPD (Fig. 3). The upper halocline (UHC) is derived from PW inflow, and it lies on top of the LHC, with its core identified by high silicate concentration (Jones and Anderson, 1986; Fig. S3). Atmospheric forcing creates the anticyclonic (i.e., convergent) Beaufort Gyre in the Canada Basin (Fig.1; Morison et al., 2021), deepening the nutricline and chlorophyll maximum in the Canada Basin interior (McLaughlin et al., 2010). This anticyclonic circulation of surface waters is also found in the UHC of the Canada Basin, while the LHC seems to share a cyclonic circulation pattern with the Atlantic layer (Pasqualini 2021).

4.1. Distribution of terrigenous DOM (tDOM)

Fluvial discharge is an important source of DOM to the Arctic Ocean (Opsahl et al., 1999; Amon, 2004; Walker et al., 2013; Anderson and Amon, 2015; Holmes et al., 2019). In the Amundsen and Makarov Basins, the concentrations of tDOM indicators were elevated in the upper 70 meters, the waters most heavily influenced by the TPD (Fig. 3). Besides the humic-like components of terrigenous and marine origin, the protein-like fluorescence exhibited a high correlation with the lignin concentration (Fig. 4). This is explained by the fact that tannins and lignins, known for their protein-binding capability, can contribute to the protein-like fluorescence signature (Maie et al., 2008).

The terrigenous contribution to DOM distinguishes the Arctic Ocean from other oceans (Anderson and Amon, 2015), as reflected in the strong correlation between DOC and lignin phenols ($rr=0.91$, $p<0.001$). *In situ* CDOM fluorescence had a similar correlation with lignin phenol concentrations as with DOC (Fig. 4b). The correlation between lignin phenols and f_{Met}

was weaker in the Canada Basin than in the Amundsen, Makarov and Nansen Basins (Fig. 4a, b), indicating that fluvial discharge plays a more prominent role in the DOM pool within the TPD and on the Eurasian side of the TPD. *In situ* CDOM fluorescence is a powerful, high vertical resolution and real-time indicator of the TPD location. The broad distribution of this current feature between the Lomonosov and Alpha Ridges shown here was also observed in 1998, 2005 (unpublished data), and 2007 (Williford et al., 2021).

The Arctic shelves, particularly the Chukchi shelf, are characterized by elevated seasonal primary productivity where sediments can serve as a source of diagenetically altered DOM (Cooper et al., 2005). The water fractions combined with the fluorescent components of DOM indicate to lateral shelf - basin transport. The UHC contains up to 100% of $f_{Pac,}$ and the LHC contains up to 85% of f_{Atl} (Fig. 2). The UHC exhibits a higher brine content (up to 5% negative SIM, indicative of excess brine) than the LHC, but both have a more negative f_{SIM} compared to the PML and the AW. Elevated concentrations of the sediment-derived fluorophores $C1_{402}$ and $C2_{404}$ (Chen et al., 2018; Williford et al., 2021) were observed in the UHC. This signal likely originates from marine organic matter decomposition in surface sediments on the shelf, consistent with a significant correlation between $C1_{402}$ fluorescence intensity and DIC concentration in the Canada Basin ($r=0.7$, $p<0.001$). The UHC showed a pronounced CDOM signature but low lignin and other tDOM proxy concentrations and high nutrient and DIC concentrations (Fig. 3), the latter two indicating organic matter degradation in source waters. The depth-integrated levels of *in situ* CDOM fluorescence and DOC concentration are lower in the LHC than in the UHC, but they are high compared to AW. The concentration of marine component $C2_{411}$ was higher in the UHC compared to the LHC, but the concentration of the terrigenous component $C2_{456}$ was higher in the LHC relative to the UHC.

The terrigenous signal in the LHC and the LHC/UHC interface suggests lateral transport of organic matter from the Eurasian shelves into the interior Arctic via the lower halocline formation process. Lignin phenol concentrations and *in situ* CDOM fluorescence peaked at the UHC/LHC interface (σ = 27.6 kg/m^3). The *in situ* CDOM fluorescence signal closely follows the density structure in the water column (Fig. 3), indicating that physical processes (e.g., sea ice formation/melt processes) have a major effect on the DOM distribution in the Arctic Ocean.

In the Western Arctic, the PML of the Canada Basin was depleted in tDOM indicators. The Beaufort Gyre alters the biogeochemical conditions of the PML layer in the Canada Basin. The layer contains up to 5% of ice melt but is dominated by the f_{Pac} (McLaughlin et al., 2004). According to the oxygen isotope and salinity calculations, the Canada Basin PML also contained up to ~16% of meteoric water, often explained by river discharge (Jones et al., 2008; Yamamoto-Kawai et al. 2008, 2009; Jensen et al., 2019; Proshutinsky et al., 2019). However, a direct riverine source is not supported, given the low concentrations of lignin phenols and fluorescent terrigenous proxies. The river water must have undergone at least one sea-ice formation/melting cycle that diminished the tDOM signal. The Mackenzie River input is mostly exported to the Archipelago, only entering the central Arctic occasionally (approximately once every 4 years; Fichot et al., 2013). The DOC concentrations were relatively high in the PML compared to halocline waters, but *in situ* CDOM fluorescence was very low (Fig. 3), indicating the presence of non-fluorescent substances in surface waters of the Canada Basin, which are mostly of marine origin (Wang et al., 2006; Shen et al., 2016).

4.2. Processes affecting the distribution of DOM in the Arctic Ocean

We consolidated data from all water masses, and the *in situ* CDOM fluorescence correlates better with f_{SIM} than with f_{Met} (r=-0.6, r=0.5, respectively, p<0.001, Fig.5), despite the fact that fluvial discharge is the largest source of CDOM to the Arctic Ocean (Amon 2004; Walker et al., 2009; Stedmon et al., 2011; Anderson and Amon, 2015; Williford et al., 2021). The correlation between f_{SIM} and *in situ* CDOM shows that sea ice formation/melt processes largely control the distribution of DOM in the Arctic Ocean, consistent with a recent study by Hölemann et al. (2021) who demonstrate that fluvial discharge is rapidly diluted by the melting of land fast ice during the spring freshet. In addition, river water undergoes at least one freeze-melt cycle on the Arctic shelf seas before entering the TPD. The mean residence time of river-runoff on the Siberian shelves is about 5±2 years (Schlosser et al., 1994). During the shelf transition, the water is imprinted with a specific oxygen isotope and salinity signature that is later carried into the central basins of the Arctic Ocean, mostly in the TPD region. The difference in negative f_{SIM} between section A, crossing the Arctic Ocean at the North Pole, and section B, situated closer to the Eurasian shelves, is likely due to the pulsed release of shelf water within the TPD system (Bauch et al., 2011; Karcher et al., 2012; Thibodeau et al., 2014; Thibodeau and Bauch, 2015; Kaiser et al., 2017).

The strongest correlation between f_{Met} and lignin phenol concentrations was observed in the TPD region of the Amundsen and Makarov Basins (r= 0.96, r=0.92, respectively; $p < 0.001$; Fig. 66). A weaker correlation was found between lignin phenols and f_{Met} in the Nansen Basin (Fig. S4). No correlations between these parameters were observed in the Chukchi Sea and the Canada Basin. The strong negative correlation between the f_{SIM} and lignin phenols in the central Arctic basins (Makarov and Amundsen) indicates substantial modification of river discharge on

the Eurasian shelves during the freezing/melting/mixing processes before entering the open Arctic Ocean. This modification of Eurasian shelf water during sea-ice formation is reflected in elevated brine fractions (negative f_{SIM} values) along with high CDOM concentrations in the TPD (Fig. 2, 3, 5) and the halocline layers. Due to the very low salinity (high buoyancy) of the PML over the shelves, most of the tDOM-enriched brine is advected above the Atlantic layer. The general overlap of the in situ CDOM trace with the iso-contour lines of brine enrichment (fraction of sea ice) is a strong testament that the distribution of DOM, originating on the Arctic shelf seas, is at least partially controlled by sea ice formation and results in lateral advection of shelf DOM to the central Arctic Ocean. Such a mechanism has been suggested by Hölemann et al. (2021), who demonstrated that typical river signals on the Eurasian shelf are diluted and overlayered by freshwater from melting fast ice. All these processes on Arctic shelves also influence the distribution of trace metals that are complexed with dissolved organic ligands. As the Arctic warms, the sea-ice cycle over the shelves has already begun to change dramatically (Li et al. 2021). In the near term, the amplitude of the annual sea-ice freeze/melt cycle might increase along with brine formation. The impacts of these changes on Arctic productivity, carbon dioxide sequestration, and TE transport need to be monitored with repeat sampling campaigns.

Basin	Pearson's correlation with fSIM	Pearson's correlation with fMet
Chukchi Shelf	-0.56	non-significant
Canada Basin	-0.59	non-significant
Makarov Basin	-0.78	0.76
Amundsen Basin	-0.79	0.85
Nansen Basin	-0.88	non-significant
All basins	-0.6	0.5

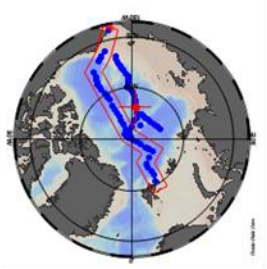

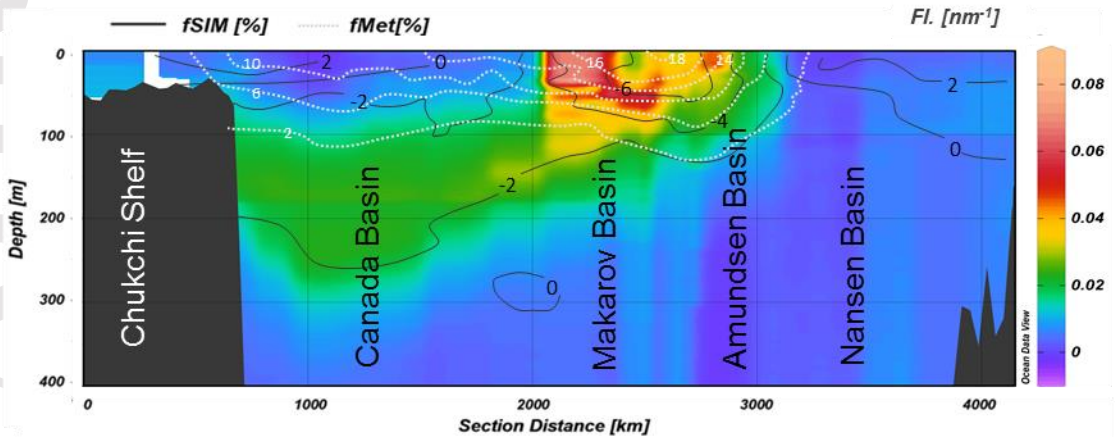

Figure 6. Top panel: relationship (Pearson correlation) of the *in situ* CDOM fluorescence (Fl.), with f_{SIM} and f_{Met} in the top 400 meters of the Chukchi Sea, Canada, Makarov, Amundsen, and Nansen Basins. Only significant ($p < 0.001$) correlations are shown. Bottom panel: the *in situ* CDOM fluorescence for section A in the upper 400 m. The light gray dotted lines represent the f_{Met} isolines, and the solid black lines represent f_{SIM} isolines.

4.3. Trace metals in relation to DOM and hydrographic features

The external sources controlling the TE distributions in the GN01 and GN04 Arctic GEOTRACES sections have been presented previously (Jensen et al., 2019, 2020; Zhang et al., 2019; Gerringa et al., 2021; Fig. 55, S5, S6). Nonetheless, one of the goals of this study was to compare the distributions of TEs with those of DOM components in order to understand how organics might control TE distributions in the Arctic Ocean. Several factors are known to control the relationship between DOM and TE distributions. First, the long-distance transport of low-

solubility trace metals, e.g., Fe(III), heavily depends on complexation with organic ligands (Gledhill and Buck, 2012). In other cases, high correlation of the trace metal and DOM indicators can point to a common source and transportation mechanisms, e.g., Mn(II) is present in free form in seawater (Byrne, 2002; Jensen et al., 2020), so it does not depend on binding to organic ligands to maintain solubility. Weak correlations between DOM and dissolved metals do not necessarily mean weak trace element-organic ligands associations, as, for example, the concentration of available ligands can greatly exceed the concentration of TEs. In addition, processes such as biological uptake and remineralization may affect the correlations between DOM and dissolved metals concentrations.

In the Central Arctic (TPD waters), lignin phenol concentrations, as well as optical indicators of terrigenous DOM ($C1_{482}$, $C2_{492}$), showed strong correlations with dFe and dCu (Fig. 44, S7) and a moderate correlation with dNi (Fig. S7) due either to strong binding to terrigenous ligands within the DOM pool or a common point of origin and co-transport mechanisms.

The dFe correlation with DOC was lower than that with lignin (Fig. 44), indicating preferential binding of dFe with terrigenous DOM. Previous studies have shown the association of dFe with humic-like terrigenous organic ligands, particularly in the TPD, and humic-like marine ligands (Laglera et al., 2019). Slagter et al. (2019) reported that humic substances are, in fact, the dominant type of Fe-binding organic ligand in the surface of the Arctic Ocean. While dFe and divalent dCu are known to be organically complexed in natural waters (Slagter et al., 2017, 2019; Laglera et al., 2019; Williford et al., 2021; Semeniuk et al 2015, Shank et al., 2004), the organic chelation of dNi is less well understood (Vraspir & Butler, 2009). It appears that dNi can be partially complexed by strong organic ligands (logK=17-19; Van den Berg and Nimmo, 1987; Morel et al., 2003). Terrestrial humic substances have been suggested as the likely source

of high-affinity, low abundance ligands for dCu (Muller and Batchelli, 2013). Another study reported that fluvial allochthonous organic matter dominated the strong complexation capacity of dCu in the Cape Fear River estuary (Shank et al., 2004). Indeed, compared to Fe and Ni, Cu likely prefers sulfur-containing ligands of lower molecular weight (Zhengbin et al., 1982). While we cannot know for sure that the correlations between the TEs and the organic compounds mean organic complexation, their strong correlations certainly warrant further investigation of the organic ligand binding of these riverine-derived metals as well as their behavior during sea ice formation. Other trace metals (dZn, dMn, dCd) did not appear to be transported across the TPD by tDOM binding.

The optical sediment signal ($C1_{402}$) showed moderate correlations with dFe, dNi, and dCu (Fig. S8). The former, dFe, dissipated rapidly within the UHC moving offshore, while dNi, dCu, and $C1_{402}$ concentrations persisted in the central Canada Basin (Fig. S5, S6). In the Chukchi Sea, brine rejection drives convection, creating dense, metal- and organic-rich bottom waters, which detrain from the shelf, feed the UHC, and spread along isopycnals across the Canada Basin (Mathis et al., 2007). The degraded shelf-derived DOM serves as a source of ligands to the UHC. The dZn (Jensen et al., 2019), dCd (Zhang et al., 2019), dCu, dNi (Jensen et al., 2022), and dMn (Jensen et al., 2020) have elevated concentrations throughout the UHC in the Canada Basin water column (Fig. S5, S6). The strong correlation of dCd, dZn, and dNi with $C1_{402}$ in the Canada Basin suggests the Chukchi shelf sediments are an important source of trace metals (Fig. S8) as well as a source of strong organic ligands that bind to them and carry them offshore within the UHC. Indeed, in previous studies, dZn was shown to be strongly complexed (>95%) by organic ligands (Jakuba et al., 2012), especially sedimentary humic acids (Sohn and Hughes 1981; Raspor et al., 1984) and low-molecular-weight thiols (Dupont and Ahner 2005). Less is

known about the potential organic ligands that bind to dCd, but prior studies have found that ~70% of the dCd in surface waters was strongly complexed (Bruland 1992).

Dissolved Cu was the only trace metal to exhibit a significant correlation with DOC concentrations and protein-like fluorescence in the upper 300 meters of the Canada Basin (Fig. S7) and a negative correlation with DIC (Fig. S8), suggesting dCu is likely complexed with marine DOM in the Canada Basin, consistent with previous findings that DOM derived from marine phytoplankton and cyanobacteria could be an important source of Cu ligands (Laglera & van den Berg 2003; Nixon et al., 2019). Coccolithophorids release thiols in response to Cu addition (Croot et al., 2000), and thiol-like levels were associated with the chlorophyll-*a* maximum in the Canadian Archipelago and Canada Basin (Gao and Guéguen, 2018; Nixon et al., 2019). The high correlation between f_{Met} and dCu, but not between dCu and CDOM, is evidence that the river water had been through at least one freezing cycle before reaching the Beaufort Gyre (there was no correlation between the lignin phenols concentrations and the f_{Met} in the Canada Basin). That is to say that the sea-ice formation/melting cycle in the Canada Basin strips out the tDOM signal, but the dCu content seems to be conserved due to the availability of algal-derived ligands, as indicated by the high correlation with DOC.

The scavenging-prone dFe and dMn are rapidly lost, moving away from the continental slope (Fig. S5, S6, Jensen, et al. 2020). Dissolved Fe exhibits weak to absent complexation to degraded UHC marine DOM molecules, as opposed to a strong correlation to tDOM within the TPD current (Williford et al., 2021). Besides scavenging, dFe concentrations in the Canada Basin are moderated by light- and nitrate-limited biological uptake (Aguilar-Islas et al., 2013). Dissolved Mn shares common sources and sinks with dFe but has a different redox reactivity and speciation

(Middag et al., 2011; Jensen et al., 2020). The correlations of dMn with *in situ* CDOM fluorescence, DOC, and lignin phenols were positive but statistically insignificant. As mentioned above, in contrast to dFe, whose solubility depends on organic complexation, most dMn in seawater is considered to exist in the free form (Byrne, 2002). In estuaries, dMn does not undergo significant salt-initiated coagulation or precipitation (Sholkovitz and Copland, 1981), but it is subject to bacterial precipitation (Sunda, 2012). Recent studies, however, show that humic ligands may play a greater role in dMn transport from coastal areas to the ocean than previously thought (Oldham et al., 2017, 2020).

The LHC exhibits relatively low concentrations of TEs (Fig. S5, S6; Gerringa et al., 2021) and similarly had low concentrations of DOM (Fig. 2). The Eurasian shelves are generally deeper and less biologically productive than the Chukchi Sea shelf, reducing the amount of remineralized and diagenetically altered organic matter released from sediments (Jones and Anderson, 1986; Sakshaug 2004). However, these shelves receive large amounts of terrigenous DOM, which might mask autochtonous DOM release from the sediments (Rijkenberg et al., 2018).

5. Conclusions

DOM is a valuable tracer of water masses and features of the Arctic Ocean. In the Amundsen and Makarov Basins, the concentration of tDOM was elevated in the upper 70 m of the water column due to the Transpolar Drift. In contrast to the central Arctic basins, the PML of the Canada and Nansen Basins was depleted in tDOM. Underneath the PML, the UHC in the Canada Basin was marked by high DIC concentrations and a Chukchi-shelf-sediment-derived signature. The terrigenous signal found in the LHC and LHC/UHC interface demonstrates the lateral

transport of organic matter from the Eurasian shelves into the Arctic interior via an advective lower halocline formation process. Sea-ice formation and melting processes shape the patterns of DOM distributions relative to hydrography and water mass tracers by separating DOM from river water. This has consequences for the interpretation of coupled physical/biogeochemical driving factors influencing source assignments for freshwater, DOM, carbon, as well as trace metal/DOM interactions.

The distributions and co-variation of TEs and DOM indicators in the Arctic Ocean provided novel insights about the complex interactions of marine biogeochemical cycles, potential metal-ligand interactions, and sea-ice formation and melting. Chukchi shelf sediments were the most important sources of dCd, dZn, and dNi, as well as sediment-derived organic ligands that bind and carry them offshore within the UHC in the Canada Basin. In contrast, dCu was associated with marine DOM in the PML and the UHC of the Canada Basin. Sediment-derived DOM did not appear to facilitate the long-range spreading of dFe into the UHC in the Canada Basin. On the other hand, tDOM molecules were found to be strong ligands for dFe, dNi, and dCu, facilitating their long-range transport from the Eurasian shelves to the central Arctic Ocean via the TPD system and eventually the East Greenland Current and the North Atlantic as suggested by the distribution of terrigenous CDOM in these waters (Amon et al., 2003) and a recent study in the Fram Strait (Krisch et al 2022).

Qualitative DOMstudies, e.g. nuclear magnetic resonance (NMR), coupled with hydrography and trace metal distributions are necessary to further constrain biological utilization and growth as well as physical processes, such as freezing/thawing, advection, and particle scavenging. This study highlights the importance of understanding the biogeochemistry of DOM and its potential

to provide insights about water mass transformations, freshwater sources, and the fate of TEs in the Arctic Ocean.

Acknowledgments

We thank the captain and crew of the RV Polarstern and USCGC Healy, the chief scientists, Ursula Schauer and the late David Kadko, for leadership, and Martin Fleisher for sampling on the Healy. Funding came from the US NSF Office of Polar Programs grant 1504469 (RMWA, RB, KK) and NSF OCE 1536506 (KK and RMWA), 1713677 (JNF) and 1436748 (DAH). MAG was supported by the former Centre for Ice, Climate and Ecosystems at the Norwegian Polar Institute. LJAG was supported by the Dutch NWO under contract number 822.01.018. We also acknowledge the international GEOTRACES Steering Committee, the U.S. GO-SHIP program, and all GEOTRACES colleagues who facilitated this extensive geochemical Arctic Ocean dataset. Polarstern and the expedition PS94 are acknowledged by Knust (2017) and AWI_PS94_00, respectively.

Data Availability Statement

The data collected during the U.S. Arctic GEOTRACES (GN01; Kadko and Landing, 2015) cruise are available in a consolidated form as part of the GEOTRACES Intermediate Data Product 2021, at https://www.geotraces.org/geotraces-intermediate-data-product-2021/.
The data collected during the GEOTRACES TransARC II cruise (PS94; Rabe et al., 2016a, 2016b; Schauer, 2016) can be found at the PANGAEA data archive (https://www.pangaea.de: https://doi.org/10.1594/PANGAEA.859558), the British Oceanographic Data Centre (http://www.bodc.ac.uk/geotraces), and Biological and Chemical Oceanography Data Management Office (Landing et al., 2019a, 2019b).
The DOC data are available online (Hansell, 2017; 2021).
Dissolved Fe and other TE data were obtained from Jensen et al., (2019) for GN01 Zn, Zhang et al., (2020) for GN01 Cd, Jensen et al., (2019, 2020, 2022) for GN01 Fe and Mn, Gerringa et al., and Jensen (2022) for GN01 Cu and Ni.
The isotope data were from Pasqualini et al., (2017) and Paffrath et al., (2021).

References

Aguilar-Islas, A. M., Rember, R., Nishino, S., Kikuchi, T., & Itoh, M. (2013). Partitioning and lateral transport of iron to the Canada Basin. Polar Science, 7(2), 82-99.

Ahmed, R., Prowse, T., Dibike, Y., Bonsal, B., & O'Neil, H. (2020). Recent trends in freshwater influx to the Arctic Ocean from four major Arctic-draining rivers. Water, 12(4), 1189.

Alkire, M. B., Rember, R., & Polyakov, I. (2019). Discrepancy in the identification of the Atlantic/Pacific front in the central Arctic Ocean: NO versus nutrient relationships. Geophysical Research Letters, 46, 3843–3852. https://doi.org/10.1029/2018GL081837

Amon, R.M.W, G. Budeus & B. Meon. 2003. Dissolved organic carbon (DOC) distribution and origin in the Nordic Seas: Exchanges with the Arctic Ocean and the North Atlantic. J. Geophys. Res.-Oceans: Vol. 108, No. C7,3221,doi:10.1029/2002JC001594.

Amon, R. M. W., 2004. The role of dissolved organic matter for the Arctic Ocean carbon cycle, In "The Arctic Ocean Organic Carbon Cycle: Present and Past", R. Stein, R.W. Macdonald, Eds., pp. 83-99. Springer.

Amon, R. M. W., Rinehart, A. J., Duan, S., Louchouarn, P., Prokushkin, A., Guggenberger, G., ... & McClelland, J. W. (2012). Dissolved organic matter sources in large Arctic rivers. Geochimica et Cosmochimica Acta, 94, 217-237.

Anderson L. G., Andersson P. S., Björk G., Peter Jones E., Jutterström S. and Wahlström I. (2013) Source and formation of the upper halocline of the Arctic Ocean. J. Geophys. Res. Oceans 118, 410–421.

Anderson, L. G., & Amon, R. M. W., (2015). DOM in the Arctic Ocean. In Biogeochemistry of marine dissolved organic matter, pp. 609-63 Academic Press

Bauch, D., van der Loeff, M. R., Andersen, N., Torres- Valdes, S., Bakker, K., & Abrahamsen, E. P. (2011). Origin of freshwater and polynya water in the Arctic Ocean halocline in summer 2007. Progress in Oceanography, 91(4), 482–495. https://doi.org/10.1016/J.POCEAN.2011.07.017

Benner, R., (2011). Loose ligands and available iron in the ocean. Proceedings of the National Academy of Sciences, 108, 3, 893-894.

Benner, R., Louchouarn, P., & Amon, R. M. W. (2005). Terrigenous dissolved organic matter in the Arctic Ocean and its transport to surface and deep waters of the North Atlantic. Global Biogeochemical Cycles, 19(2).

Berner, L. T., Massey, R., Jantz, P., Forbes, B. C., Macias-Fauria, M., Myers-Smith, I., ... & Goetz, S. J. (2020). Summer warming explains widespread but not uniform greening in the Arctic tundra biome. Nature communications, 11(1), 1-12.

Bruhwiler, L., Parmentier, F. J. W., Crill, P., Leonard, M., & Palmer, P. I. (2021). The arctic carbon cycle and its response to changing climate. Current Climate Change Reports, 7(1), 14-34.

Bruland, K. W. (1992). Complexation of cadmium by natural organic ligands in the central North Pacific. Limnology and Oceanography, 37(5), 1008-1017.

Butler, A., & Theisen, R. M. (2010). Iron (III)–siderophore coordination chemistry: Reactivity of marine siderophores. Coordination chemistry reviews, 254(3-4), 288-296.

Byrne, R. H. (2002). Speciation in seawater. Chemical speciation in the Environment, 322-357.

Carmack, E. C., Yamamoto- Kawai, M., Haine, T. W., Bacon, S., Bluhm, B. A., Lique, C., ... & Williams, W. J. (2016). Freshwater and its role in the Arctic Marine System: Sources, disposition, storage, export, and physical and biogeochemical consequences in the Arctic and global oceans. Journal of Geophysical Research: Biogeosciences, 121(3), 675-717.

Carmack, E., McLaughlin, F., Yamamoto-Kawai, M., Itoh, M., Shimada, K., Krishfield, R., & Proshutinsky, A. (2008). Freshwater storage in the Northern Ocean and the special role of the Beaufort Gyre. In Arctic–subArctic ocean fluxes (pp. 145-169). Springer, Dordrecht.
Charette, M. A., Kipp, L. E., Jensen, L. T., Dabrowski, J. S., Whitmore, L. M., Fitzsimmons, J. N., et al., 2020. The Transpolar Drift as a source of riverine and shelf- derived trace elements to the central Arctic Ocean. Journal of Geophysical Research: Oceans, 125, e2019JC015920. https://doi.org/10.1029/2019JC015920
Chen, M., Jung, J., Lee, Y. K., & Hur, J. (2018). Surface accumulation of low molecular weight dissolved organic matter in surface waters and horizontal off-shelf spreading of nutrients and humic-like fluorescence in the Chukchi Sea of the Arctic Ocean. Science of the Total Environment, 639, 624-632.
Cooper, L. W., Benner, R., McClelland, J. W., Peterson, B. J., Holmes, R. M., Raymond, P. A., ... & Codispoti, L. A. (2005). Linkages among runoff, dissolved organic carbon, and the stable oxygen isotope composition of seawater and other water mass indicators in the Arctic Ocean. Journal of Geophysical Research: Biogeosciences, 110(G2).
Cory, R. M., Miller, M. P., McKnight, D. M., Guerard, J. J., & Miller, P. L. (2010). Effect of instrument- specific response on the analysis of fulvic acid fluorescence spectra. Limnology and Oceanography: Methods, 8(2), 67-78.
Croot PL, Moffett JW, Brand LE. (2000) Production of extracellular Cu complexing ligands by eucaryotic phytoplankton in response to Cu stress. Limnol Oceanogr. 2000;45:619–27.
Cutter, G. A., Andersson, P. S., Codispoti, L., Croot, P. L., Francois, R., Lohan, M. C., et al., (2014). Sampling and Sample-handing Protocols for GEOTRACES Cruises. Retrieved from http://www.geotraces.org/images/stories/documents/intercalibration/Cookbook_v2.pdf
Dupont CL, Ahner BA. (2005) Effects of copper, cadmium, and zinc on the production and exudation of thiols by Emiliania huxleyi. Limnol Oceanogr. 2005;50:508–15.
Fichot, C. G., Kaiser, K., Hooker, S. B., Amon, R. M., Babin, M., Bélanger, S., ... & Benner, R. (2013). Pan-Arctic distributions of continental runoff in the Arctic Ocean. Scientific reports, 3(1), 1-6.
Fritz, M., Vonk, J. E., & Lantuit, H. (2017). Collapsing arctic coastlines. Nature Climate Change, 7(1), 6-7.
Gao, Z., & Guéguen, C. (2018). Distribution of thiol, humic substances and colored dissolved organic matter during the 2015 Canadian Arctic GEOTRACES cruises. Marine Chemistry, 203, 1-9.
Gerringa, L. J. A., Rijkenberg, M. J. A., Slagter, H. A., Laan, P., Paffrath, R., Bauch, D., ... & Middag, R. (2021). Dissolved Cd, Co, Cu, Fe, Mn, Ni, and Zn in the Arctic Ocean. Journal of Geophysical Research: Oceans, 126(9), e2021JC017323.
Gerringa, Loes J A; Rijkenberg, Micha J A; Slagter, Hans A (2018): Dissolved iron measured on board with Flow injection analysis and iron-binding dissolved organic ligands from Ultra Clean CTD collected depth profiles during GEOTRACES PS94 Arctic cruise on Polarstern. PANGAEA, https://doi.org/10.1594/PANGAEA.890975
Gledhill, M., & Buck, K. N. (2012). The organic complexation of iron in the marine environment: a review. Frontiers in microbiology, 3, 69.
Gonçalves-Araujo, R., Granskog, M. A., Bracher, A., Azetsu-Scott, K., Dodd, P. A., & Stedmon, C. A. (2016). Using fluorescent dissolved organic matter to trace and distinguish the origin of Arctic surface waters. Scientific Reports, 6(1), 33978. https://doi.org/10.1038/srep33978

Gonçalves- Araujo, R., Stedmon, C. A., de Steur, L., Osburn, C. L., & Granskog, M. A. (2020). A decade of annual Arctic DOC export with Polar Surface Water in the East Greenland Current. Geophysical Research Letters, 47(20), e2020GL089686.
Gonçalves-Araujo, R., Stedmon, C. A., Heim, B., Dubinenkov, I., Kraberg, A., Moiseev, D., & Bracher, A. (2015). From fresh to marine waters: Characterization and fate of dissolved organic matter in the Lena River Delta Region, Siberia. Frontiers in Marine Science, 2, 108.
Guay, C. K., McLaughlin, F. A., & Yamamoto- Kawai, M. (2009). Differentiating fluvial components of upper Canada Basin waters on the basis of measurements of dissolved barium combined with other physical and chemical tracers. Journal of Geophysical Research: Oceans, 114(C1).
Guéguen, C., Itoh, M., Kikuchi, T., Eert, J., and Williams, W. J. (2015). Variability in dissolved organic matter optical properties in surface waters in the Amerasian Basin. Front. Mar. Sci. 2:78. https://doi.org/10.3389/fmars.2015.00078
Haine, T.W.N., Curry, B., Gerdes, R., Hansen, E., Karcher, M., Lee, C., Rudels, B., Spreen, G., de Steur, L., Stewart, K.D., Woodgate, R., (2015). Arctic freshwater export: Status, mechanisms, and prospects. Glob. Planet. Change 125, 13–35. doi:10.1016/j.gloplacha.2014.11.013
Halewood, E., K. Opalk, L. Custals, M. Carey, D.A. Hansell, & C.A. Carlson. (2010). GO-SHIP Repeat Hydrography: Determination of dissolved organic carbon (DOC) and total dissolved nitrogen (TDN) in seawater using High Temperature Combustion Analysis. In The GO-SHIP Repeat Hydrography Manual: A Collection of Expert Reports and Guidelines. Hood, E.M., C.L. Sabine, and B.M. Sloyan, eds. IOCCP Report Number 14, ICPO Publication Series Number 134. http://www.go-ship.org/HydroMan.html.
Hansell, D. A. (2005). Dissolved organic carbon reference material program.Eos, Transactions American Geophysical Union,86(35), 318. https://doi.org/10.1029/2005EO350003
Hansell, D.A. (2021). DOC data from Cruise 33HQ20150809, exchange version. Accessed from CCHDO https://cchdo.ucsd.edu/cruise/33HQ20150809. Access date 2021-03-27. CCHDO cruise DOI: 10.7942/C2MW25.
Hansell, Dennis A (2017): Arctic dissolved organic carbon (DOC) and total dissolved nitrogen (TDN) collected during POLARSTERN cruise PS94 (GEOTRACES) in 2015. Rosenstiel School of Marine & Atmospheric Sciences, University of Miami, PANGAEA, https://doi.org/10.1594/PANGAEA.884113
Hertkorn, N., Benner, R., Frommberger, M., Schmitt-Kopplin, P., Witt, M., Kaiser, K.,...,.
Hedges, J.I (2006), Characterization of a major refractory component of marine dissolved organic matter. Geochimica et Cosmochimica Acta, 70 (12), pp. 2990-3010
Hölemann, J. A., Juhls, B., Bauch, D., Janout, M., Koch, B. P., & Heim, B. (2021). The impact of land-fast ice on the distribution of terrestrial dissolved organic matter in the Siberian Arctic shelf seas. Biogeosciences Discussions, 1-30.
Holmes, R. M., McClelland, J. W., Tank, S. E., Spencer, R. G. M., & Shiklomanov, A. I. (2019). Arctic Great Rivers Observatory. Water Quality Dataset, Version 20190904. Retrieved from https://arcticgreatrivers.org/data
Horner-Devine, A. R., Hetland, R. D., & MacDonald, D. G. (2015). Mixing and transport in coastal river plumes. Annual Review of Fluid Mechanics, 47, 569-594.
Jackson, J. M., E. C. Carmack, F. A. McLaughlin, S. E. Allen, and R. G. Ingram (2010), Identification, characterization, and change of the near-surface temperature maximum in the Canada Basin, 1993-2008, J. Geophys. Res., 115, doi:10.1029/2009JC005265.

Jakuba, R. W., Saito, M. A., Moffett, J. W., & Xu, Y. (2012). Dissolved zinc in the subarctic North Pacific and Bering Sea: Its distribution, speciation, and importance to primary producers. Global Biogeochemical Cycles, 26, GB2015. https://doi.org/10.1029/2010GB004004
Jensen, L. T., Cullen, J.T., Jackson, S.L., Gerringa, L.J., Bauch, D., Middag, R., Sherrell R.M., Fitzsimmons, J.N., (2022), A refinement of the processes controlling dissolved copper and nickel biochemistry: insights from the pan-Arctic. Journal of Geophysical Research: Oceans: e2021jc018087.
Jensen, L. T., N. J. Wyatt, B. S. Twining, S. Rauschenberg, W. M. Landing, R. M. Sherrell, and J. N. Fitzsimmons (2019), Biogeochemical Cycling of Dissolved Zinc in the Western Arctic (Arctic GEOTRACES GN01), Global Biogeochemical Cycles, 33(3), 343-369.
Jensen, L. T., P. Morton, B. S. Twining, M. I. Heller, M. Hatta, C. I. Measures, S. John, R. Zhang, P. Pinedo-Gonzalez, and R. M. Sherrell (2020), A comparison of marine Fe and Mn cycling: US GEOTRACES GN01 Western Arctic case study, Geochimica et Cosmochimica Acta.
Jiang, W., Gastineau, G., & Codron, F. (2021). Multicentennial variability driven by salinity exchanges between the atlantic and the arctic ocean in a coupled climate model. Journal of Advances in Modeling Earth Systems, 13(3), e2020MS002366.
Jones, E. P., & Anderson, L. G. (1986). On the origin of the chemical properties of the Arctic Ocean halocline. Journal of Geophysical Research: Oceans, 91(C9), 10759-10767.
Jones, E. P., Anderson, L. G., Jutterström, S., Mintrop, L., & Swift, J. H. (2008). Pacific freshwater, river water and sea ice meltwater across Arctic Ocean basins: Results from the 2005 Beringia Expedition. Journal of Geophysical Research: Oceans, 113(C8).
Kadko, D., & Landing, W. (2015). U.S. Arctic GEOTRACES USCGC Healy (HLY1502) cruise report. Retrieved from https://www.bodc.ac.uk/resources/inventories/cruise_inventory/reports/healy1502.pdf
Kaiser, K., Benner, R., & Amon, R. M. W. (2017). The fate of terrigenous dissolved organic carbon on the Eurasian shelves and export to the North Atlantic. Journal of Geophysical Research, Oceans, 122, 4–22. https://doi.org/10.1002/2016JC012380
Karcher, M., Smith, J. N., Kauker, F., Gerdes, R., & Smethie, W. M. (2012). Recent changes in Arctic Ocean circulation revealed by iodine- 129 observations and modeling. Journal of Geophysical Research: Oceans, 117(C8).
Kikuchi, T., Hatakeyama, K., and Morison, J. H. (2004), Distribution of convective Lower Halocline Water in the eastern Arctic Ocean, J. Geophys. Res., 109, C12030, doi:10.1029/2003JC002223.
Krisch, S., Hopwood, M. J., Roig, S., Gerringa, L. J. A., Middag, R., Rutgers van der Loeff, M. M., et al. (2022). Arctic – Atlantic exchange of the dissolved micronutrients iron, manganese, cobalt, nickel, copper and zinc with a focus on Fram Strait. Global Biogeochemical Cycles, 36, e2021GB007191. https://doi.org/10.1029/2021GB007191
Klunder, M. B., Laan, P., Middag, R., De Baar, H. J. W., & Bakker, K. (2012). Dissolved iron in the Arctic Ocean: Important role of hydrothermal sources, shelf input and scavenging removal. Journal of Geophysical Research: Oceans, 117(C4).
Knust, R. (2017). Polar Research and Supply Vessel POLARSTERN Operated by the Alfred-Wegener-Institute. Journal of large-scale research facilities, 3, A119. http://dx.doi.org/10.17815/jlsrf-3-163
Kondo, Y., Obata, H., Hioki, N., Ooki, A., Nishino, S., Kikuchi, T., & Kuma, K. (2016). Transport of trace metals (Mn, Fe, Ni, Zn and Cd) in the western Arctic Ocean (Chukchi Sea and

Canada Basin) in late summer 2012. Deep Sea Research Part I: Oceanographic Research Papers, 116, 236-252.
Korhonen, M., Rudels, B., Marnela, M., Wisotzki, A., & Zhao, J. (2013). Time and space variability of freshwater content, heat content and seasonal ice melt in the Arctic Ocean from 1991 to 2011. Ocean Science, 9(6), 1015-1055.
Kothawala, D. N., Stedmon, C. A., Müller, R. A., Weyhenmeyer, G. A., Köhler, S. J., & Tranvik, L. J. (2014). Controls of dissolved organic matter quality: Evidence from a large- scale boreal lake survey. Global change biology, 20(4), 1101-1114. https://doi.org/10.1111/gcb.12488
Krachler, R., von der Kammer, F., Jirsa, F., Süphandag, A., Krachler, R. F., Plessl, C., ... & Hofmann, T. (2012). Nanoscale lignin particles as sources of dissolved iron to the ocean. Global Biogeochemical Cycles, 26(3).
Laglera, L. M., & van den Berg, C. M. (2003). Copper complexation by thiol compounds in estuarine waters. Marine Chemistry, 82(1-2), 71-89.
Laglera, L. M., and van den Berg, C. M. G. (2009). Evidence for geochemical control of iron by humic substances in seawater. Limnol. Oceanogr. 54, 610–619. doi: 10.4319/lo.2009.54.2.0610
Laglera, L.M., Sukekava, C., Slagter, H.A., Downes, J., Aparicio-Gonzalez, A., Gerringa, L.J.A., (2019). First Quantification of the Controlling Role of Humic Substances in the Transport of Iron Across the Surface of the Arctic Ocean. Environ. Sci. Technol.
Landing, W. M., Cutter, G., & Kadko, D. C. (2019b). Bottle data from the GEOTRACES clean carousel sampling system (GTC) on the Arctic section cruise (HLY1502) from August to October 2015 (U.S. GEOTRACES Arctic project). Biological and Chemical Oceanography Data Management Office (BCO- DMO). https://doi.org/10.1575/1912/bco- dmo.647259.4
Li, H., Fedorov, A., & Liu, W. (2021). AMOC stability and diverging response to Arctic sea ice decline in two climate models. Journal of Climate, 34(13), 5443-5460.
Maie, N., Pisani, O., & Jaffé, R., (2008). Mangrove tannins in aquatic ecosystems: their fate and possible influence on dissolved organic carbon and nitrogen cycling. Limnology and Oceanography, 53, 1, 160-171.
Makarewicz, A., Kowalczuk, P., Sagan, S., Granskog, M. A., Pavlov, A. K., Zdun, A., ... & Zabłocka, M. (2018). Characteristics of chromophoric and fluorescent dissolved organic matter in the Nordic Seas. Ocean Science, 14(3), 543-562
Mathis, J. T., Pickart, R. S., Hansell, D. A., Kadko, D., & Bates, N. R. (2007). Eddy transport of organic carbon and nutrients from the Chukchi Shelf: Impact on the upper halocline of the western Arctic Ocean. Journal of Geophysical Research: Oceans, 112(C5).
McLaughlin, F. A., & Carmack, E. C. (2010). Deepening of the nutricline and chlorophyll maximum in the Canada Basin interior, 2003–2009. Geophysical Research Letters, 37(24).
McLaughlin, F. A., E. C. Carmack, R. W. Carmack, H. Macdonald, J. H.Melling, P. A. Swift, B. F. Wheeler, and E. B. Sherr (2004), The joint roles of Pacific and Atlantic-origin waters in the Canada Basin, 1997–1998, Deep Sea Res., Part I, 51, 107 – 128, doi:1 0.1016/j.dsr.20009.010.
Metzner, E. P., Salzmann, M., & Gerdes, R. (2020). Arctic Ocean surface energy flux and the cold halocline in future climate projections. Journal of Geophysical Research: Oceans, 125(2), e2019JC015554.
Middag, R., de Baar, H. J. W., Laan, P., and Klunder, M. B., (2011). Fluvial and hydrothermal input of manganese into the Arctic Ocean. Geochim. Cosmochim. Acta 75, 2393– 2408. doi: 10.1016/j.gca.2011.02.011.
Morel, F. M., & Price, N. M. (2003). The biogeochemical cycles of trace metals in the oceans. Science, 300(5621), 944-947.

Morison, J., Kwok, R., Dickinson, S., Andersen, R., Peralta-Ferriz, C., Morison, D., ... & Guthrie, J. (2021). The Cyclonic Mode of Arctic Ocean Circulation. Journal of Physical Oceanography.
Muller, F. L., & Batchelli, S. (2013). Copper binding by terrestrial versus marine organic ligands in the coastal plume of River Thurso, North Scotland. Estuarine, Coastal and Shelf Science, 133, 137-146.
Murphy, K. R., Stedmon, C. A., Graeber, D., and Bro, R. (2013). Fluorescence spectroscopy and multi-way techniques. PARAFAC. Anal. Methods 5, 6557. https://doi.org/10.1039/c3ay41160e
Murphy, K. R., Stedmon, C. A., Wenig, P., & Bro, R. (2014). OpenFluor–an online spectral library of auto-fluorescence by organic compounds in the environment. Analytical Methods, 6(3), 658-661.
Nakayama, Y., Fujita, S., Kuma, K., & Shimada, K. (2011). Iron and humic- type fluorescent dissolved organic matter in the Chukchi Sea and Canada Basin of the western Arctic Ocean. Journal of Geophysical Research: Oceans, 116(C7).
Newton, R., Schlosser, P., Mortlock, R., Swift, J., & MacDonald, R. (2013). Canadian Basin freshwater sources and changes: Results from the 2005 Arctic Ocean Section. Journal of Geophysical Research: Oceans, 118(4), 2133-2154.
Nishimura, S., Kuma, K., Ishikawa, S., Omata, A., & Saitoh, S. I. (2012). Iron, nutrients, and humic- type fluorescent dissolved organic matter in the northern Bering Sea shelf, Bering Strait, and Chukchi Sea. Journal of Geophysical Research: Oceans, 117(C2).
Nixon, R. L., Jackson, S. L., Cullen, J. T., & Ross, A. R. (2019). Distribution of copper-complexing ligands in Canadian Arctic waters as determined by immobilized copper (II)-ion affinity chromatography. Marine Chemistry, 215, 10367
Oldham, V. E., Lamborg, C. H., & Hansel, C. M. (2020). The spatial and temporal variability of Mn speciation in the coastal northwest Atlantic Ocean. Journal of Geophysical Research: Oceans, 125(1), e2019JC015167.
Oldham, V. E., Mucci, A., Tebo, B. M., & Luther III, G. W. (2017). Soluble Mn (III)–L complexes are abundant in oxygenated waters and stabilized by humic ligands. Geochimica et Cosmochimica Acta, 199, 238-246.
Opsahl, S., & Benner, R., (1997). Distribution and cycling of terrigenous dissolved organic matter in the ocean. Nature, 386, 6624, 480.
Opsahl, S., Benner, R., Amon, R. M. W., (1999): Major flux of terrigenous dissolved organic matter through the Arctic Ocean. Limnology & Oceanography: 44: 2017-2023
Paffrath, R., Laukert, G., Bauch, D., van der Loeff, M. R., & Pahnke, K. (2021). Separating individual contributions of major Siberian rivers in the Transpolar Drift of the Arctic Ocean. Scientific Reports, 11(1), 1-11.
Pasqualini, A., Schlosser, P., Newton, R., & Koffman, T. N. (2017). U.S. GEOTRACES Arctic section ocean water hydrogen and oxygen stable isotope analyses (version 1.0) [dataset]. Interdisciplinary Earth Data Alliance (IEDA). https://doi.org/10.1594/ieda/100633
Pearson, R. G. (1963). Hard and soft acids and bases. Journal of the American Chemical society, 85(22), 3533-3539.
Paqualini, A., (2021). Circulation pathways, time scales, and water mass composition in the Arctic Ocean: Results from 25 years of tracer observations. Dissertation, Columbia University Libraries, NY, USA. https://doi.org/10.7916/d8-8a0m-9n67
Pokrovsky, O. S., Viers, J., Dupre, B., Chabaux, F., Gaillardet, J., Audry, S., ... & Shevchenko, V. P. (2012). Biogeochemistry of carbon, major and trace elements in watersheds of northern

Eurasia drained to the Arctic Ocean: the change of fluxes, sources and mechanisms under the climate warming prospective. Comptes Rendus Geoscience, 344(11-12), 663-677.
Polyakov, I. V., Bhatt, U. S., Walsh, J. E., Abrahamsen, E. P., Pnyushkov, A. V., and Wassmann, P. F. (2013). Recent oceanic changes in the Arctic in the context of long-term observations. Ecol. Appl. 23, 1745–1764. doi: 10.1890/11-0902.1
Proshutinsky, A. Y., & Johnson, M. A. (1997). Two circulation regimes of the wind- driven Arctic Ocean. Journal of Geophysical Research: Oceans, 102(C6), 12493-12514.
Proshutinsky, A., Krishfield, R., & Timmermans, M. L. (2020). Introduction to special collection on Arctic Ocean modeling and observational synthesis (FAMOS) 2: Beaufort Gyre phenomenon. Journal of Geophysical Research: Oceans, 125(2), e2019JC015400.
Proshutinsky, A., Krishfield, R., Toole, J. M., Timmermans, M. L., Williams, W., Zimmermann, S., ... & Zhao, J. (2019). Analysis of the Beaufort Gyre freshwater content in 2003–2018. Journal of Geophysical Research: Oceans, 124(12), 9658-9689.
Rabe, B., Karcher, M., Kauker, F., Schauer, U., Toole, J. M., Krishfield, R. A., ... & Su, J. (2014). Arctic Ocean basin liquid freshwater storage trend 1992–2012. Geophysical Research Letters, 41(3), 961-968.
Rabe, B., Karcher, M., Kauker, F., Schauer, U., Toole, J.M., Krishfield, R.A., Pisarev, S., Kikuchi, T., Su, K., (2014) "Arctic Ocean liquid freshwater storage trend 1992-2012", Geophys. Res. Lett., 41(3),961-968, doi:10.1002/2013GL058121
Rabe, Benjamin; Schauer, Ursula; Ober, Sven; Horn, Myriel; Hoppmann, Mario; Korhonen, Meri; Pisarev, Sergey; Hampe, Hendrik; Villacieros, Nicolas; Savy, Jean Philippe; Wisotzki, Andreas (2016a): Physical oceanography during POLARSTERN cruise PS94 (ARK-XXIX/3). Alfred Wegener Institute, Helmholtz Centre for Polar and Marine Research, Bremerhaven, PANGAEA, https://doi.org/10.1594/PANGAEA.859558
Rabe, Benjamin; Schauer, Ursula; Ober, Sven; Horn, Myriel; Hoppmann, Mario; Korhonen, Meri; Pisarev, Sergey; Hampe, Hendrik; Villacieros, Nicolas; Savy, Jean Philippe; Wisotzki, Andreas (2016b): Physical oceanography measured on water bottle samples during POLARSTERN cruise PS94 (ARK-XXIX/3). Alfred Wegener Institute, Helmholtz Centre for Polar and Marine Research, Bremerhaven, PANGAEA, https://doi.org/10.1594/PANGAEA.859559
Raspor, B., Nürnberg, H. W., Valenta, P., & Branica, M. (1984). Studies in seawater and lake water on interactions of trace metals with humic substances isolated from marine and estuarine sediments: II. Voltammetric investigations on trace metal complex formation in the dissolved phase. Marine Chemistry, 15(3), 231-249.
Rennermalm, A. K., Wood, E. F., Déry, S. J., Weaver, A. J., & Eby, M. (2006). Sensitivity of the thermohaline circulation to Arctic Ocean runoff. Geophysical research letters, 33(12).
Rijkenberg, Micha J A; Slagter, Hans A; Rutgers van der Loeff, Michiel M; van Ooijen, Jan C; Gerringa, Loes J A (2018): Dissolved Fe in the Deep and Upper Arctic Ocean With a Focus on Fe Limitation in the Nansen Basin. Frontiers in Marine Science, 5, https://doi.org/10.3389/fmars.2018.00088
Rudels, B. (2009). Arctic ocean circulation. Academic Press.
Rudels, B. (2015). Arctic Ocean circulation, processes and water masses: A description of observations and ideas with focus on the period prior to the International Polar Year 2007–2009. Progress in Oceanography, 132, 22-67.
Rudels, B., (2001). Ocean Current: Arctic Basin Circulation. In J. Steele, S. Thorpe, & K. Turekian, Eds., Encyclopedia of Ocean Sciences, pp. 177-187

Rudels, B., Anderson, L. G., Jones, E. P., (1996). Formation and evolution of the surface mixed layer and halocline of the Arctic Ocean. J. Geophys. Res. 101, 8807-8821.
Rudels, B., Korhonen, M., Schauer, U., Pisarev, S., Rabe, B., & Wisotzki, A. (2015). Circulation and transformation of Atlantic water in the Eurasian Basin and the contribution of the Fram Strait inflow branch to the Arctic Ocean heat budget. Progress in Oceanography, 132, 128-152.
Sakshaug E. (2004) Primary and Secondary Production in the Arctic Seas, The Organic Carbon Cycle in the Arctic Ocean. Springer, pp. 57–81.
Schauer, U. (2016). The Expedition PS94 of the research vessel POLARSTERN to the central Arctic Ocean in 2015, Bremerhaven, Alfred Wegener Institute for Polar and Marine Research. Berichte zur Polar- und Meeresforschung = Reports on polar and marine research 703 170 pp.
Schlitzer, R. (2020). Ocean Data View, ODV 5.2. 1.
Schlosser, P., Bauch, D., Fairbanks, R., & Bönisch, G. (1994). Arctic river-runoff: mean residence time on the shelves and in the halocline. Deep Sea Research Part I: Oceanographic Research Papers, 41(7), 1053-1068.
Semeniuk, D. M., Bundy, R. M., Payne, C. D., Barbeau, K. A., & Maldonado, M. T. (2015). Acquisition of organically complexed copper by marine phytoplankton and bacteria in the northeast subarctic Pacific Ocean. Marine Chemistry, 173, 222-23
Shank, G. C., Skrabal, S. A., Whitehead, R. F., & Kieber, R. J. (2004). Strong copper complexation in an organic-rich estuary: the importance of allochthonous dissolved organic matter. Marine Chemistry, 88(1-2), 21-39.
Shen, Y., Benner, R., Robbins, L. L., & Wynn, J. G. (2016). Sources, distributions, and dynamics of dissolved organic matter in the Canada and Makarov Basins. Frontiers in Marine Science, 3, 198.
Shimada, K., Carmack, E. C., Hatakeyama, K., & Takizawa, T. (2001). Varieties of shallow temperature maximum waters in the western Canadian Basin of the Arctic Ocean. Geophysical Research Letters, 28(18), 3441-3444.
Sholkovitz, E. R., & Copland, D. (1981). The coagulation, solubility and adsorption properties of Fe, Mn, Cu, Ni, Cd, Co and humic acids in a river water. Geochimica et Cosmochimica Acta, 45(2), 181-189.
Slagter, H. A., Reader, H. E., Rijkenberg, M. J. A., Van Der Loeff, M. R., de Baar, H. J. W., & Gerringa, L. J. A. (2017). Organic Fe speciation in the Eurasian Basins of the Arctic Ocean and its relation to terrestrial DOM. Marine Chemistry, 197, 11-25.
Slagter, H.A., Laglera, L.M., Sukekava, C., Gerringa, L.J.A., (2019). Fe-Binding Organic Ligands in the Humic-Rich TransPolarDrift in the Surface Arctic Ocean Using Multiple Voltammetric Methods. J. Geophys. Res. Ocean. 1491–1508.
Sohn, M. L., & Hughes, M. C. (1981). Metal ion complex formation constants of some sedimentary humic acids with Zn (II), Cu (II) and Cd (II). Geochimica et Cosmochimica Acta, 45(12), 2393-2399.
Stedmon, C. A., Amon, R. M. W., Bauch, D., Bracher, A., Gonçalves- Araujo, R., Hoppmann, M., et al., (2021). Insights Into Water Mass Origins in the Central Arctic Ocean From In- Situ Dissolved Organic Matter Fluorescence. Journal of Geophysical Research: Oceans, 126(7), e2021JC017407. https://doi.org/10.1029/2021JC017407
Stedmon, C. A., Amon, R. M. W., Rinehart, A. J., & Walker, S. A. (2011a). The supply and characteristics of colored dissolved organic matter (CDOM) in the Arctic Ocean: Pan Arctic trends and differences. Marine Chemistry, 124(1–4), 108–118. https://doi.org/10.1016/J.MARCHEM.2010.12.007

Stedmon, C. A., Granskog, M. A., & Dodd, P. A. (2015). An approach to estimate the freshwater contribution from glacial melt and precipitation in East Greenland shelf waters using colored dissolved organic matter (CDOM). Journal of Geophysical Research: Oceans, 120(2), 1107–1117. https://doi.org/10.1002/2014JC010501
Stedmon, C. A., Thomas, D. N., Papadimitriou, S., Granskog, M. A., & Dieckmann, G. S. (2011b). Using fluorescence to characterize dissolved organic matter in Antarctic sea ice brines. Journal of Geophysical Research: Biogeosciences, 116(G3).
Sunda, W. G. (2012). Feedback interactions between trace metal nutrients and phytoplankton in the ocean. Frontiers in microbiology, 3, 204
Thibodeau, B., & Bauch, D. (2015). River Water and Brine Inventory over the Laptev Sea Shelf: 2007 To 2011. In AGU Fall Meeting Abstracts (Vol. 2014, pp. OS51C-1005).
Thibodeau, B., Bauch, D., Kassens, H., & Timokhov, L. A. (2014). Interannual variations in river water content and distribution over the Laptev Sea between 2007 and 2011: The Arctic Dipole connection. Geophysical Research Letters, 41(20), 7237-7244.
Ulfsbo, A., Jones, E. M., Casacuberta, N., Korhonen, M., Rabe, B., Karcher, M., & Van Heuven, S. M. (2018). Rapid changes in anthropogenic carbon storage and ocean acidification in the intermediate layers of the Eurasian Arctic Ocean: 1996–2015. Global Biogeochemical Cycles, 32(9), 1254-1275.
Van den Berg, C. M. G., & Nimmo, M. (1987). Determination of interactions of nickel with dissolved organic material in seawater using cathodic stripping voltammetry. Science of the Total Environment, 60, 185-195.
Vraspir, J. M., and A. Butler (2009), Chemistry of marine ligands and siderophores.
Walker, S. A., Amon, R. M. W., and Stedmon, C. A. (2013). Variations in high-latitude riverine fluorescent dissolved organic matter: a comparison of large Arctic rivers. J. Geophys. Res. Biogeosci. 118, 1689–1702. https://doi.org/10.1002/2013jg002320
Walker, S.A., Amon, R. M. W., Stedmon, C., Duan, S.W. Louchouarn, P., (2009). The use of PARAFAC modeling to trace terrestrial dissolved organic matter and fingerprint water masses in coastal Canadian Arctic surface waters. J. Geophys. Res. 114, https://doi.org/10.1029/2009jg000990
Wang, D., Henrichs, S. M., & Guo, L. (2006). Distributions of nutrients, dissolved organic carbon and carbohydrates in the western Arctic Ocean. Continental Shelf Research, 26(14), 1654-1667.
Watanabe, E. (2013). Linkages among halocline variability, shelf-basin interaction, and wind regimes in the Beaufort Sea demonstrated in pan-Arctic Ocean modeling framework. Ocean Modelling, 71, 43-5
Whitmore, L. M., Pasqualini, A., Newton, R., & Shiller, A. M. (2020). Gallium: A new tracer of Pacific Water in the Arctic Ocean. Journal of Geophysical Research: Oceans, 125(7), e2019JC015842.
Williford, T., Amon, R. M. W., Benner, R., Kaiser, K., Bauch, D., Stedmon, C., ... & Klunder, M. B. (2021). Insights into the origins, molecular characteristics and distribution of iron-binding ligands in the Arctic Ocean. Marine Chemistry, 103936.
Woodgate, R. A., Weingartner, T. J., & Lindsay, R. (2012). Observed increases in Bering Strait oceanic fluxes from the Pacific to the Arctic from 2001 to 2011 and their impacts on the Arctic Ocean water column. Geophysical Research Letters, 39(24).

Woosley, R. J., Millero, F. J., & Takahashi, T. (2017). Internal consistency of the inorganic carbon system in the Arctic Ocean. Limnology and Oceanography: Methods, 15(10), 887–896. https://doi.org/10.1002/lom10208

Yamamoto- Kawai, M., McLaughlin, F. A., Carmack, E. C., Nishino, S., & Shimada, K. (2008). Freshwater budget of the Canada Basin, Arctic Ocean, from salinity, δ18O, and nutrients. Journal of Geophysical Research: Oceans, 113(C1).

Yamamoto- Kawai, M., McLaughlin, F. A., Carmack, E. C., Nishino, S., Shimada, K., & Kurita, N. (2009). Surface freshening of the Canada Basin, 2003–2007: River runoff versus sea ice meltwater. Journal of Geophysical Research: Oceans, 114(C1).

Yamashita, Y., Boyer, J. N., & Jaffé, R. (2013). Evaluating the distribution of terrestrial dissolved organic matter in a complex coastal ecosystem using fluorescence spectroscopy. Continental shelf research, 66, 136-144.

Yan, G., & Kaiser, K., (2018a). A rapid and sensitive method for the analysis of lignin phenols in environmental samples using ultra-high performance liquid chromatography-electrospray ionization-tandem mass spectrometry with multiple reaction monitoring. Analytica chimica acta, 1023, 74-80.

Yan, G., K. Kaiser., (2018b). Ultra-low Sample Volume Cupric Sulfate Oxidation Method for the Analysis of Dissolved Lignin. Anal. Chem., https://DOI.org/10.1021/acs.analchem.8b01867, 68, 1-2, 59-70

Zhang, P., Wu, Z., & Jin, R. (2021). How can the winter North Atlantic Oscillation influence the early summer precipitation in Northeast Asia: Effect of the Arctic sea ice. Climate Dynamics, 56(5), 1989-2005.

Zhang, R., Jensen, L. T., Fitzsimmons, J. N., Sherrell, R. M., & John, S. (2019). Dissolved cadmium and cadmium stable isotopes in the western Arctic Ocean. Geochimica et Cosmochimica Acta, 258, 258-27

Zhengbin, Z., & Liansheng, L. (1982). Microcosmic approach to marine chemistry—A Φ (Z/l, x) rule of chemical processes in seawater and its applications. Chinese Journal of Oceanology and Limnology, 1(1), 54-75.

Zhong, W., & Zhao, J. (2014). Deepening of the Atlantic Water core in the Canada Basin in 2003–11. Journal of Physical Oceanography, 44(9), 2353-2369.